

1

2 ***COOLAIR* and *PRC2* function in parallel to silence *FLC* during vernalization**

3

4

5 Mathias Nielsen[†], Govind Menon[†], Yusheng Zhao, Eduardo Mateo-Bonmati, Philip Wolff, Shaoli Zhou,
6 Martin Howard* & Caroline Dean*

7 John Innes Centre, Norwich Research Park, Norwich NR4 7UH, UK

8 [†]These authors contributed equally to this work

9 *Corresponding authors Caroline Dean and Martin Howard

10 Email: caroline.dean@jic.ac.uk; martin.howard@jic.ac.uk

11 ORCID (C.D.): 0000-0002-6555-3525

12 Author contributions: MN, YZ, EM-B, PW, SZ performed the experimental work and analysed the data,
13 GM undertook the modelling, MH and CD supervised the work; MN, GM, MH, CD wrote the
14 manuscript.

15 There are no competing interests

16 Classification: Biological Sciences: Plant Biology

17 Keywords: antisense transcription; Polycomb Repressive Complex 2, *FLC*, Arabidopsis

18 This PDF includes:

19 Main text

20 Figures 1-4

21

22 **Abstract**

23 Non-coding transcription induces chromatin changes that can mediate environmental responsiveness, but
24 the causes and consequences of these mechanisms are still unclear. Here, we investigate how antisense
25 transcription (termed *COOLAIR*) interfaces with Polycomb Repressive Complex 2 silencing during
26 winter-induced epigenetic regulation of Arabidopsis *FLOWERING LOCUS C (FLC)*. We use genetic and
27 chromatin analyses on lines ineffective or hyperactive for the antisense pathway in combination with
28 computational modelling to define the mechanisms underlying *FLC* repression. Our results show that
29 *FLC* is silenced through pathways that function with different dynamics: a *COOLAIR* transcription-
30 mediated pathway capable of fast response; and in parallel a slow Polycomb Repressive Complex 2
31 (PRC2) switching mechanism that maintains each allele in an epigenetically silenced state. Components
32 of both the *COOLAIR* and PRC2 pathways are regulated by a common transcriptional regulator (NTL8),
33 which accumulates by reduced dilution due to slow growth at low temperature. The parallel activities of
34 the regulatory steps, and their control by temperature-dependent growth dynamics, create a flexible
35 system for registering widely fluctuating natural temperature conditions that change year on year, and yet
36 ensure robust epigenetic silencing of *FLC*.

37

38 **Significance statement**

39 The role of non-coding transcription in chromatin regulation is still controversial. This controversy has
40 extended to the role of transcription of antisense transcripts called *COOLAIR* in the Polycomb-mediated
41 epigenetic silencing of Arabidopsis *FLC*, a key step in the process of vernalization. Here, we show that
42 *COOLAIR* transcription and PRC2 silence *FLC* in parallel pathways; an antisense-mediated
43 transcriptional repression capable of fast response, and a slow PRC2 epigenetic silencing, both of which
44 are affected by growth dynamics and temperature fluctuations. These features explain the varied
45 importance of *COOLAIR* transcription in cold-induced *FLC* epigenetic silencing seen in various studies
46 using different conditions. The parallel repressive inputs and extensive feedbacks make the mechanism
47 counter-intuitive but provide great flexibility to the plant.

48 **Main text**

49 **Introduction**

50 Non-coding transcription has emerged as an important mechanism in environmentally responsive gene
51 regulation. In some cases non-coding transcription induces chromatin changes that are lost if the
52 environmental signal is removed (1, 2). In other cases chromatin changes, particularly those involving the
53 Polycomb mark H3K27me3, are epigenetically maintained providing a memory of the inductive signal.
54 One well-characterised example of the latter is the winter-induced epigenetic silencing of the Arabidopsis

55 floral repressor gene, *FLC* (3, 4). This underpins the vernalization process, the acceleration of flowering
56 by winter exposure. The process includes early induction of a series of antisense transcripts, called
57 *COOLAIR* (5); a slow epigenetic switch from an active chromatin environment (marked by H3K36me3)
58 to a silenced chromatin state (marked by H3K27me3) at an internal three nucleosome region (6); and
59 spreading of the H3K27me3 Polycomb silencing over the whole locus (7-8). The switching mechanism
60 involves canonical Polycomb Repressive Complex 2 (PRC2) and Arabidopsis PRC2 accessory proteins
61 VIN3 and VRN5. VIN3 is slowly induced by cold exposure (9), interacts with PRC2 at the nucleation
62 region downstream of the *FLC* transcription start site, and has a functionally important head-to-tail
63 polymerization domain (10).

64

65 The timing of early antisense transcription and later VIN3 expression led to the view that antisense
66 transcription was a prerequisite for PRC2 silencing. Consistent with this, single-molecule FISH
67 experiments revealed that *COOLAIR* expression was mutually exclusive with *FLC* sense transcription at
68 each allele (11). This sequence of events was initially tested through T-DNA insertions into the
69 *COOLAIR* promoter. These had little effect on long-term vernalization (12). Similarly, *FLC* silencing was
70 unaffected in studies using a CRISPR deletion of the *COOLAIR* promoter or mutation of *CBF* factors,
71 known to facilitate cold-induction of *COOLAIR* (13). However, replacement of *COOLAIR* 5' sequences
72 (TEX1 line) attenuated *FLC* transcriptional silencing and disrupted the co-ordinated changes in
73 H3K36me3 and H3K27me3 occurring at the *FLC* nucleation region (14).

74

75 *COOLAIR* had much stronger effects in experiments analysing *FLC* silencing in natural field conditions.
76 *COOLAIR* expression was strongly induced on the first freezing night of autumn (15, 16), a result re-
77 created in controlled environment cabinets (15). In these experiments, one freezing night was sufficient to
78 induce *COOLAIR*, but several freezing nights were required to silence *FLC*, with silencing attenuated by
79 disruption of antisense transcription. This data is reminiscent of many *S. cerevisiae* loci, where non-
80 coding transcription plays an important role in environmental responsiveness (1, 17, 18). However,
81 extensive feedback mechanisms between chromatin, transcription and co-transcriptional processes make
82 functions of non-coding transcription difficult to elucidate. In particular, buffering between transcription
83 and RNA stability leads to changed transcriptional dynamics with no change in steady state RNA (2).

84

85 To clarify the regulatory mechanism at Arabidopsis *FLC*, we have undertaken a series of genetic,
86 molecular, and computational analyses to investigate the role of *COOLAIR* in cold-induced *FLC*
87 silencing. Here, we show that *FLC* is silenced through parallel pathways. *COOLAIR* transcription can
88 limit sense transcription, and this is associated with reduction in levels of the active histone mark

89 H3K36me3; this mechanism involves disruption of a 5'-3' *FLC* gene loop. In parallel, PRC2 silencing
90 switches each allele from an epigenetically ON to an OFF state; this involves nucleation of H3K27me3
91 and subsequent spreading over the locus during subsequent growth, associated with further reduction in
92 H3K36me3 (6). The nucleated and spread states differentially influence *FLC* transcription, which is still
93 modulated by *COOLAIR* transcription. While *FLC* silencing by the PRC2 pathway operates on a slow
94 timescale, the rapid induction capability of *COOLAIR* transcription, as seen in freezing conditions (15),
95 enables this pathway in these conditions to silence *FLC* transcription on fast timescales. Components of
96 both pathways are also regulated by their common transcriptional regulator NTL8 (19), which
97 accumulates based on reduced dilution dependent on growth dynamics in the different cold phases. We
98 integrate these parallel regulatory activities into a mathematical model that predicts *FLC* chromatin
99 dynamics and transcription in different conditions. We argue that parallel activities converging onto a
100 common target provides great flexibility in gene regulation, providing responsiveness to a wide variety of
101 conditions. There are extensive similarities between how antisense transcription modulates *FLC* and how
102 it alters sense transcription dynamics in yeast (2).

103

104 **Results**

105 ***COOLAIR* rather than PRC2 nucleation is the major contributor to *FLC* repression in *ntl8-D3*.** Two
106 independent genetic screens in different genotypes had identified dominant mutations that revealed NTL8
107 regulates *VIN3* and *COOLAIR* (15, 19). Ectopic *COOLAIR* expression leads to very low *FLC* levels in
108 warm grown plants (15). We therefore confirmed that *VIN3* and *COOLAIR* are both misregulated in the
109 dominant mutant *ntl8-D3* (Fig. 1A), and then used it to genetically activate both pathways
110 simultaneously, independently of cold. *FLC* transcriptional output, histone modifications and chromatin
111 topology were analysed. Paralleling cold effects on wild-type plants the ectopic *COOLAIR* expression in
112 *ntl8-D3* resulted in a clear decrease in H3K36me3, as compared to *ColFRI*, at the *FLC* transcription start
113 site (TSS) and over the gene body (Fig. 1B). The high *COOLAIR* transcription in *ntl8-D3* led to
114 accumulation of H3K36me3 at the *COOLAIR* promoter (Fig. 1B), matching the cold-induced transient
115 increase of H3K36me3 in *ColFRI* at the same position. The decrease in H3K36me3 was not accompanied
116 by an increase in H3K27me3 observed during vernalization (Fig. 1C). Likewise, H2Aub, another histone
117 modification that accumulates at *FLC* during early vernalization did not accumulate ectopically in *ntl8-*
118 *D3* (Fig. 1D). The lack of accumulation of H3K27me3 and H2Aub in *ntl8-D3* compared to *ColFRI* in the
119 absence of cold supports the view that *VIN3* expression itself is not sufficient to cause Polycomb
120 mediated silencing of *FLC*. These data indicate that antisense-mediated suppression rather than *VIN3*-
121 mediated nucleation of H3K27me3 is the major factor causing *FLC* repression in *ntl8-D3*. Repression of

122 sense *FLC* transcription in *ntl8-D3* is almost completely suppressed when *COOLAIR* transcription is
123 blocked, giving further support to this conclusion (15).

124

125 **Ectopically expressed VIN3 localises to *FLC* but fails to induce H3K27me3 nucleation.** To
126 understand what prevents the accumulation of H3K27me3 in *ntl8-D3* despite ectopic VIN3 expression,
127 we tested if other epigenetic factors are misexpressed in *ntl8-D3*. Only one of the tested genes changed
128 slightly in expression (*SI Appendix*, Fig. S1). We then analysed association of VIN3 at the nucleation
129 region in *ntl8-D3*. Despite the lack of H3K27me3 accumulation in *ntl8-D3*, we found VIN3-eGFP
130 accumulated at the *FLC* nucleation region in warm conditions, mimicking the accumulation during
131 vernalization (Fig. 1E). Thus, VIN3 accumulation at the nucleation region does not result in stable
132 nucleation of H3K27me3. To distinguish VIN3 intrinsic binding to the *FLC* nucleation region,
133 independently of *COOLAIR* transcriptional induction, we expressed VIN3-eGFP under the promoter of
134 *VRN5* (*SI Appendix*, Fig. S2A). This resulted in expression levels in non-vernalized plants that paralleled
135 VIN3 induction after six weeks cold (6WT0) (*SI Appendix*, Fig. S2B). In this line VIN3-eGFP was
136 enriched at the *FLC* locus in NV conditions (*SI Appendix*, Fig. S2C), showing VIN3 can remain
137 associated with the nucleation region even when *FLC* is strongly expressed. We found that VIN3
138 association in *ntl8-D3* led to H3K27me2 enrichment despite no accumulation of H3K27me3 (Fig. 1F).
139 Thus, cold-induced features, possibly influencing residence time, are required to enable VIN3
140 functionality to deliver H3K27me3 to the nucleation region.

141

142 **Ectopic induction of *COOLAIR* correlates with chromatin topology changes.** A cold-induced feature
143 at *FLC* is disruption of a gene loop conformation that links the transcription start site (TSS) and the
144 transcription termination site (20). In *ntl8-D3*, we found that the gene loop was ectopically disrupted,
145 mimicking vernalization (Fig. 1G). This suggests that gene loop disruption is linked with antisense-
146 mediated reduction in *FLC* transcription. We also found that the *TEX2.0* transgene, where a *nos*
147 terminator promotes early *COOLAIR* termination, reduces gene loop formation (*SI Appendix*, Fig. S3),
148 consistent with earlier reports using a similar, but not identical transgene (21). This result suggests a role
149 for the activity of the antisense promoter/TSS, rather than antisense transcription per se, as being
150 important for gene loop disruption.

151

152 **Disrupting *COOLAIR* transcription perturbs H3K27me3 dynamics before and during cold, but not**
153 **post-cold H3K27me3 levels.** We further investigated the fact that ectopic expression of antisense
154 transcription is enough to cause lower H3K36me3 around the *FLC* sense TSS and in the gene body, even

155 in the absence of cold. Antisense transcription could lower H3K36me3 levels, either through direct
156 removal mediated by antisense transcription or indirectly by limiting sense transcription, thus preventing
157 the co-transcriptional addition of H3K36 methylation. To dissect the interplay of H3K36me3 and
158 H3K27me3, we studied the dynamic changes in these modifications using a vernalization time course.

159 Our previous analyses of TEX transgenes were in an *flc-2* background, where part of the endogenous *FLC*
160 genomic sequence remains (4). This limited the regions where the chromatin modifications on the
161 transgene could be studied (14). To overcome this limitation, we generated a FRI +, *FLC* null (*flclean*)
162 where the entire *FLC* genomic sequence had been deleted using CRISPR (*SI Appendix*, Fig. S4) and
163 introduced the previously described TEX1.0 (replacement of the *COOLAIR* promoter) and TEX2.0
164 (insertion of a *nos* terminator to truncate *COOLAIR* transcription) transgenes. We also included a *FRI*
165 *FLC_{ΔCOOLAIR}* CRISPR line, which deletes the *COOLAIR* promoter at the endogenous locus (22). Using
166 these multiple defective *COOLAIR* lines and respective controls, we undertook a detailed time course of
167 histone modifications during vernalization, including multiple time points post-cold (Fig. 2A, B).

168
169 The rate of accumulation of H3K27me3 during cold exposure was not reduced in the *COOLAIR* defective
170 genotypes compared to the wild-type, and at some timepoints was even accelerated (Fig. 2C and *SI*
171 *Appendix*, Fig. S5A,B), consistent with our previous data (14). By 6WT0, wild-type and *COOLAIR*
172 defective genotypes show similar H3K27me3 levels in the nucleation region (Fig. 2A and *SI Appendix*,
173 Fig. S5C). However, there were clear differences in the starting levels of H3K27me3, being significantly
174 lower in the nucleation region in all defective *COOLAIR* genotypes (Fig. 2A and *SI Appendix*, Fig. S5D).
175 Consistent with the differences in starting H3K27me3 levels, and supporting a role for antisense
176 transcription in establishment of the initial *FLC* chromatin state (23), the defective *COOLAIR* genotypes
177 showed a consistent trend of higher *FLC* RNA before cold exposure (*SI Appendix*, Fig. S5E), although
178 the differences were small. The similar trend in TEX1, TEX2 and *FLC_{ΔCOOLAIR}* argues against this being
179 a specific TEX transgene effect. We interpret the H3K27me3 level in *ColFRI* before cold as representing
180 a fraction of *FLC* alleles that have switched to a stable Polycomb silenced state. Thus, higher H3K27me3
181 levels in *ColFRI* compared to the *COOLAIR* defective genotypes may reflect the *COOLAIR* role in
182 developmentally regulated PRC2 silencing of *FLC* (24, 25). After cold there was no significant difference
183 in H3K27me3 levels in the nucleation region between *ColFRI* and any of the *COOLAIR* defective
184 genotypes (Fig. 2A and *SI Appendix*, Fig. S5C). Spreading of H3K27me3 was also unaffected in the
185 *COOLAIR* defective genotypes, as seen from the similar levels in the gene body at 6WT10 and 6WT20
186 (Fig. 2A). Overall, we find that H3K27me3 dynamics before and during cold are perturbed by *COOLAIR*,
187 but that post-cold H3K27me3 levels are not.

188

189 **Disrupting *COOLAIR* transcription attenuates H3K36me3 removal during vernalization.**

190 H3K36me3 levels were similar in all genotypes before vernalization (Fig. 2B and *SI Appendix*, Fig. S5F)
191 but decreased at different rates during cold exposure (Fig. 2D). This contrasts with the clear NV
192 differences in H3K27me3 levels. However, this is consistent with the NV H3K27me3 levels coming from
193 a small fraction of silenced alleles, while most alleles are transcriptionally active and contribute to the
194 observed H3K36me3 levels, a scenario that generates bigger fold changes in H3K27me3 than in
195 H3K36me3, as we observe (*SI Appendix*, Fig. S5G). H3K36me3 levels reduced more slowly in all
196 defective *COOLAIR* genotypes at 6WT0 (Fig. 2B and *SI Appendix*, Fig. S5G), but after 2 weeks cold
197 H3K36me3 levels increased in the gene body compared to NV (Fig. 2B). There were no differences in
198 H3K36me3 levels between *COOLAIR* defective genotypes and wild-type *ColFRI* after transfer back to
199 warm (Fig. 2B). In *ntl8-D3*, where *VIN3* and *COOLAIR* are both overexpressed, faster reduction of
200 H3K36me3 in the cold was observed, while H3K27me3 was less affected (*SI Appendix*, Fig. S6 A-D, *SI*
201 *Appendix*, Fig. S9B-C). Together our results demonstrate that the Polycomb pathway is effective enough
202 to completely silence the *FLC* locus, despite either an ineffective or hyperactive antisense pathway. The
203 *COOLAIR*-mediated pathway mediates not only the removal of H3K36me3 but also H3K4me1 through
204 the activity of the demethylase complex FLD-LD-SDG26 (23). H3K4me1, like H3K36me3, has been
205 shown to be added co-transcriptionally in plants (26). Consistently, we found that in the *COOLAIR*
206 defective lines, H3K4me1 reduction during vernalization was attenuated (*SI Appendix*, Fig. S7) showing
207 the same trend as H3K36me3, including the increase at 2WT0. Overall, we find that *COOLAIR* defective
208 genotypes have reduced rates of H3K36me3 removal, but after cold, any differences in H3K36me3 levels
209 disappear. The relative changes of the unspliced *FLC* RNA levels did not match the corresponding
210 H3K36me3 levels in the *COOLAIR* defective genotypes and effects on spliced *FLC* levels were different
211 to unspliced (Fig. 2E-F). This suggests a similar interconnected mechanism linking chromatin
212 modification to transcript stability as found in yeast, with unspliced and spliced transcripts affected in
213 different ways (2).

214

215 **H3K27me3 accumulation is not necessary for *COOLAIR*-mediated transcriptional downregulation.**

216 A mutation in the core PRC2 component Su(z)12 (*VRN2*) only partially disrupted *FLC* repression (*SI*
217 *Appendix*, Fig. S8A) (6), whilst H3K36me3 fold reduction at *FLC* during the cold was hardly changed (*SI*
218 *Appendix*, Fig. S8B), despite accumulation of H3K27me3 being abolished (6). Thus, H3K36me3
219 reduction and *FLC* RNA downregulation do not rely on H3K27me3 nucleation. Analysis of a *vrn5-*
220 *TEX1.0* combination, defective in H3K27me3 accumulation and *COOLAIR*, had shown that the
221 H3K36me3 reduction seen in an H3K27me3 nucleation mutant is mediated by *COOLAIR* (14). To

222 examine this aspect further, we analysed changes in the two modifications, H3K36me3 and H3K27me3,
223 in fluctuating cold conditions, where we see the clearest indication of *COOLAIR* transcription regulating
224 *FLC* expression (15). Under these conditions, *COOLAIR* was highly upregulated, causing significant
225 downregulation of *FLC* sense transcript (15). Whilst we have previously shown that full-length
226 *COOLAIR* transcription is essential for the *FLC* downregulation in these conditions (15), a role for
227 H3K27me3 nucleation had not been investigated. Here we analysed H3K36me3 and H3K27me3 levels in
228 *ColFRI* at 2WT0, under three different cold conditions (as in (15)), constant 5°C (CC, Constant Cold),
229 mild 3°C - 9°C (FM, Fluctuating Mild), and strong fluctuating conditions -1°C - 12°C (FS, Fluctuating
230 Strong). Zhao et al., 2021 showed that *COOLAIR* upregulation and *FLC* downregulation were greatest in
231 the FS condition. Therefore, we would expect H3K36me3 to show the largest changes in this condition,
232 and indeed this is seen in our data (Fig. 3A, *SI Appendix*, Fig. S9E). Both mild fluctuating and constant
233 cold result in smaller changes (Fig. 3A, *SI Appendix*, Fig. S9E). In contrast, H3K27me3 accumulation
234 showed little difference between the different conditions (Fig. 3B and *SI Appendix*, Fig. S9D), indicating
235 that H3K27me3 is not the major contributor to the enhanced downregulation under strongly fluctuating
236 conditions. The lack of difference in H3K27me3 accumulation, despite the relatively large change in
237 antisense expression, further highlights the parallel and almost independent nature of these *FLC*
238 repression pathways. To further confirm that *COOLAIR* transcription is necessary for the changes in
239 H3K36me3 under fluctuating conditions, we subjected the TEX1.0 defective *COOLAIR* line to these
240 conditions. As expected, the reduction in H3K36me3 was also attenuated relative to *ColFRI* (Fig. 3C, D).
241 This is consistent with the lack of *FLC* sense transcriptional shutdown under FS conditions in a
242 *COOLAIR* deletion line as recently described (27). Interestingly, for *COOLAIR* defective genotypes, the
243 slight increase in H3K36me3 at 2WT0 observed in constant cold was also recapitulated in the FM
244 conditions. The reduction under FS conditions was significantly attenuated in TEX1.0 (*SI Appendix*, Fig.
245 S9F) and an analysis to test whether this is also the case in the *COOLAIR* deletion line is ongoing.
246 Overall, we find that *COOLAIR*-mediated transcriptional repression does not strongly depend on
247 H3K27me3 nucleation, supporting our earlier results in *ntl8-D3*. The contrasting dynamics of H3K36me3
248 and H3K27me3 under 2 weeks of fluctuating conditions further highlight the fast-response capability of
249 the antisense-mediated repression. In *ColFRI*, the changes in nucleation region H3K36me3 after only 2
250 weeks of FS conditions (Fig. 3A,C) are comparable to H3K36me3 changes after 6 weeks in constant cold
251 (Fig. 2B, *SI Appendix*, Fig. 5G). The fast response capability of *FLC* antisense transcription to
252 temperature changes is also supported by field data for *A. halleri FLC* (28). They showed that H3K4me3
253 associated with *COOLAIR* transcription at the 3' end of the *FLC* locus responds to temperature changes
254 on a much faster timescale compared to the 5' end (associated with *FLC* sense transcription), which
255 responds mainly on a slow timescale.

256

257 **Mathematical modelling of *FLC* regulation reconciles the different effects of antisense transcription**

258 **on chromatin state.** The dynamics of the two repression pathways are difficult to dissect quantitatively
259 purely through molecular experiments. We therefore turned to mathematical modelling to see how the
260 observed behaviour in *COOLAIR* defective mutants could be reconciled with our existing understanding
261 of *FLC* repression in the cold. We have previously developed and experimentally validated a
262 mathematical modelling framework describing dynamically changing fractions of active/silenced *FLC*
263 alleles and their associated histone modifications (30, 31). Here we built on this framework to develop a
264 new model, incorporating an antisense-mediated silencing component. A schematic of the model
265 developed here is shown in Fig. 3E (details in Supplementary Information- the MATLAB code used to
266 simulate the ODE model is available at <https://doi.org/10.5281/zenodo.10257997>). The model was built
267 based on our main conclusion from the above data: namely that two pathways work in parallel to silence
268 *FLC*, antisense transcription and PRC2 nucleation. We then interrogated the model to see whether it was
269 capable of quantitatively reproducing histone modification dynamics in *ColFRI* and the various mutants.

270

271 The effect of the antisense-mediated pathway on sense transcription was modelled implicitly as a cold-
272 dependent graded modulator of sense initiation/transition to productive elongation. This is consistent with
273 high antisense transcription in *ntl8-d* mutants causing low levels of *FLC* transcription, independently of
274 H3K27me3 nucleation. This is also consistent with previous data showing that sense and antisense
275 transcription at *FLC* are anti-correlated in *ColFRI*, both in warm (32) and in cold conditions (11). This
276 may be through a mutual exclusivity model for the *FLC* locus, similar to that reported for the *CBF1-*
277 *SVALK*A locus, where full-length sense transcription is inhibited by antisense transcription (33). Another
278 key aspect of the model is the co-transcriptional delivery of the H3K36me3 modifications. Changes in Pol
279 II elongation behaviour can affect the H3K36me3 profile across mammalian genes (34), with slower Pol
280 II speed allowing a larger window of opportunity for adding H3K36me3 at any given location. Any
281 changes in transcription at *FLC* may be expected to produce corresponding changes in H3K36me3.
282 However, to explain the *increase* in gene body H3K36me3 observed in the defective *COOLAIR* lines,
283 specifically at 2WT0 compared to NV, despite the lack of any increase in transcriptional output over that
284 time period (Fig. 2E), the model includes a cold-induced reduction in Pol II speed in this region, resulting
285 in a longer dwell time. The SDG8 H3K36 methyltransferase, which we have shown co-transcriptionally
286 associates with RNA PolIII (29), is likely mediating these H3K36me3 changes. The model also allows for
287 H3K36me3 removal on a timescale consistent with the experimentally observed lifetime of H3K36
288 methylation in other systems (35), so that its levels at the nucleation region would decay quickly in the

289 absence of sense transcription. The model also describes dynamic changes in *FLC* mRNA levels as
290 modelled in (30). However, due to the highly variable behaviour of spliced *FLC* RNA observed in the
291 different *COOLAIR* defective mutants (Fig. 2F), which potentially reflects changes in RNA stability, we
292 do not try to capture these levels using the model.

293
294 We also incorporate the PRC2 pathway and how it silences *FLC* through H3K27me3 accumulation
295 during vernalization. In cells which can have active or non-active cell cycles, we consider that *FLC* alleles
296 can be in three different states; non-nucleated (without H3K27me3 nucleation), nucleated, and spread,
297 with the latter only attained in active cycling cells (31). To generate reasonable fits to our data,
298 particularly the higher levels of H3K36me3 observed during cold in *COOLAIR* defective mutants, we
299 found that an extension to our previous models was needed, where we allow for different levels of *FLC*
300 transcription in the three states: highest in non-nucleated, much lower in nucleated and even lower in
301 spread. Satisfactory fits also necessitated that the non-nucleated and nucleated states be capable of further
302 downregulation by antisense transcription. Consistent with the possibility of some limited transcriptional
303 activity in the nucleated state, we, therefore, allowed for potential co-existence of H3K27me3 and
304 H3K36me3 on the same nucleosome. We then fitted the model to capture the qualitative changes in
305 H3K36me3, H3K27me3, and transcription (sense and antisense) observed in the cold for *ColFRI* and the
306 defective *COOLAIR* lines. We found that this model could capture all the qualitative features of the data
307 observed in *ColFRI* and the defective *COOLAIR* lines (Fig. 4A-D), including both the increase of
308 H3K36me3 at 2WT0 and the subsequent significantly slower reduction in H3K36me3 in the latter (Fig.
309 4A,B), as well as the reduction of H3K36me3 in the post-cold seen in all the lines (Fig.4A,B).

310
311 We then tested whether the model could capture our previous datasets by simulating other mutants that
312 affect *FLC* silencing in the cold (see previously published data (6)), including an H3K27me3 nucleation
313 mutant (e.g., *vrn2*, *vin3*), a spreading mutant (e.g., *lhp1*, *clf*). In all cases, the simulation outputs from the
314 model are qualitatively consistent with data, including the post-cold behaviour of the two histone
315 modifications (*SI Appendix*, Fig. S10A-D). Interestingly, in addition to recapitulating the behaviour
316 captured by our previous models, the new model can capture the reduction of H3K36me3 in the post-cold
317 seen in *ColFRI* - a trend that could not be previously captured (Fig. 4B). This is because the new model
318 allows for higher levels of transcription (and consequently higher H3K36me3) in a nucleated state relative
319 to a spread state.

320
321 The model also incorporates a fast timescale response in the antisense mediated pathway, which can
322 respond to temperature fluctuations (see Supplementary Information for details). Briefly, this consists of a

323 simple step increase in antisense mediated repression resulting from temperatures dropping below a
324 threshold, which is incorporated into the slower timescale increase in antisense mediated repression. The
325 fast timescale response allows the model to qualitatively capture the differences in H3K36me3 and *FLC*
326 spliced RNA between the different cold conditions CC, FM, FS (*SI Appendix*, Fig. S11). The model
327 predicts that H3K36me3 and *FLC* mRNA levels respond on a fast timescale, exhibiting oscillations in
328 response to the daily repeated temperature profiles of FM and FS conditions. While the agreement
329 between the model and experiments is overall good, the model did predict reduced H3K27me3 nucleation
330 in FS conditions, which was not observed experimentally. This discrepancy may potentially arise from
331 differences between the field conditions used to parameterise our model for H3K27me3 nucleation (30)
332 and the FS experimental conditions used here. The model predicts that antisense transcription limits
333 H3K36me3 through a graded, analog reduction in *FLC* transcription rather than by directly mediating
334 H3K36me3 removal. The increased H3K36me3 at 2WT0 in *COOLAIR* defective lines, is predicted to
335 arise from a combination of higher *FLC* sense transcription (since antisense mediated repression is
336 disrupted) and cold-induced reduction in Pol II speed in the nucleation region. In a second slower
337 response chromatin pathway involving Polycomb Repressive Complex 2 (PRC2), each allele
338 progressively switches from a non-nucleated to H3K27me3 nucleated state during the cold and then to a
339 spread H3K27me3 state during post-cold growth. The model indicates that intermediate levels of *FLC*
340 transcription in the nucleated state, which can be further downregulated by antisense transcription, can
341 explain how clear differences in H3K36me3 between defective *COOLAIR* lines and the wild-type can
342 emerge in the cold yet subsequently disappear during growth after transfer to warm conditions. In these
343 conditions, all the nucleated *FLC* alleles convert to the H3K27me3 spread state due to an active cell cycle
344 (6), regardless of H3K36me3 levels and any residual expression. Hence, in the context of vernalization,
345 the *COOLAIR* repressive pathway is most important during rather than after cold.

346

347 **Discussion**

348 Focused dissection of the mechanism underlying winter-induced *FLC* silencing has established a role for
349 antisense transcription and PRC2 activity in registration of long-term exposure to noisy environmental
350 signals (5, 15, 36, 37). However, the complexity of the mechanism, and its sensitivity to variable
351 temperature and growth parameters, has led to different studies questioning the importance of the
352 antisense transcription in cold-induced *FLC* silencing. Here, using a combination of experiments and
353 mathematical modelling, we have elucidated the role of antisense transcription and PRC2 activity as
354 parallel pathways, both leading to *FLC* silencing (Fig. 4B). The antisense-mediated pathway involves the
355 *FLC* gene loop and represses *FLC* transcription (38). Two other lncRNAs have been described at *FLC*,
356 *COLDWRAP* (39) and *COLDAIR* (40). We have detected cold-up-regulated *FLC* transcripts with

357 upstream transcription start sites including *COLDWRAP* that influence *FLC* expression levels but not
358 cold-induced transcriptional silencing (41); we have not found *COLDAIR* equivalents.

359

360 The multiple effects of the *COOLAIR*-mediated transcriptional pathway on H3K36me3 in the 5' region of
361 *FLC* required modelling to deconvolve fully. In the wild-type, lower transcription leads to H3K36me3
362 reduction, but this is partly hidden in defective *COOLAIR* lines in the cold through a predicted increase in
363 H3K36me3 from slower RNA PolIII speed at the 5' end of *FLC*. The slow PRC2 switch at each *FLC*
364 allele from a non-nucleated to a H3K27me3 nucleated and then spread state is associated with decreasing
365 frequencies of *FLC* transcription, consistent with previous findings of the relationship between
366 H3K27me3 and *FLC* transcription (6). Both *COOLAIR*-mediated and PRC2 pathways are affected by the
367 common transcriptional regulator NTL8, which accumulates slowly and variably dependent on reduced
368 dilution by slower growth at low temperatures (19). Our observation that in *ntl8-D3* both *COOLAIR* and
369 *VIN3* are ectopically expressed, yet the H3K27me2 modification but not H3K27me3 accumulates, implies
370 a requirement for other cold-induced factors for vernalization (42, 43). These parallel repressive activities
371 with multiple temperature inputs enables modulation of transcriptional silencing independently of robust
372 epigenetic silencing. This gives the plants great flexibility to respond to autumnal conditions that vary in
373 different geographical regions and from year to year yet ensure robust silencing. Indeed, variation in *FLC*
374 transcriptional silencing has been shown to be an important adaptive determinant in *A. thaliana*
375 accessions (16). It seems likely that similar parallel mechanisms may be involved in other seasonal
376 responses, e.g. seed and bud dormancy and germination, for similar reasons.

377

378 The chromatin changes in *COOLAIR*-defective mutants are not directly reflected in steady-state unspliced
379 and spliced *FLC* levels (Fig. 2E,F), similar to the situation in yeast (2). Which RNA stability mechanisms
380 are involved remain to be determined, but m6A methylation has been shown to influence *FLC* regulation
381 (38, 44, 45) and is enriched in the *FLC* 3' UTR. This disconnect between chromatin dynamics and steady-
382 state RNA levels is likely to have contributed to the controversy over the role of non-coding RNA in
383 chromatin regulation generally. In addition, the effective combination of parallel pathways hides effects
384 of mutations after saturating induction, e.g. mutations in CBF-binding factors (13). Another debate has
385 been over the use of transgenes to modulate *COOLAIR* expression (13), but the use here of *FLC_{ΔCOOLAIR}*
386 and *ntl8-D3* for under/overexpression of *COOLAIR* argues against this. However, future studies need to
387 generate a fully antisense null genotype, since all defective *COOLAIR* genotypes so far produced still
388 contain cryptic antisense promoters, which become more active when the endogenous *COOLAIR*
389 promoter is mutated/deleted (15). The difficulty of completely removing antisense transcription is also
390 seen in other systems (46) and suggests transcription initiation from open chromatin regions rather than

391 specific promoter elements. Such a line would not only help elucidate the role of *COOLAIR* in the cold-
392 induced silencing of *FLC*, but also in the starting *FLC* expression upon germination, a key determinant of
393 natural variation underpinning adaptation (16).

394

395 The large number of plant chromatin regulators that interact with non-coding RNAs point to an important
396 role of similar co-transcriptional mechanisms in environmental plasticity (47, 48). This is similarly true in
397 yeast (2), where antisense expression has been associated with genes that are environmentally-silenced
398 (1). Future work will address the evolutionary parallels and conservation of a mechanism enabling rapid
399 transcriptional changes and switches to epigenetic silencing in response to noisy environmental cues.

400

401 **Materials and Methods**

402 Detailed descriptions of materials and methods are provided in the SI Appendix. A brief summary is
403 provide here.

404

405 **Plant materials**

406 All mutant and transgenic lines were in the *FRI*^{sl2} background. *ntl8-D3 FRI* was described previously
407 (15). Generation of new mutant and transgenic lines are detailed in SI Appendix.

408

409 **Expression analysis**

410 RNA analysis was performed as previously described (49). Total RNA was extracted, DNase treated, and
411 cDNA was synthesised with SuperScript IV reverse transcriptase (Invitrogen). qPCR was performed
412 using SYBR Green I Master (Roche) and analysed on a LightCycler 480 machine (Roche).

413

414 **Chromatin immunoprecipitation**

415 Chromatin immunoprecipitation (ChIP) was performed as described in (49). ChIP was performed with
416 antibodies: α -H3 (Abcam, ab1791), α -H3K36me3 (Abcam, ab9050), α -H3K27me3 (Abcam, ab192985),
417 α -H3K27me2 (Upstate, 07-452), α -H2AK119ub (Cell Signaling Technology, #8240), α -H3K4me1
418 (Abcam, ab8895), and α -GFP (Abcam, ab290).

419

420 **Chromatin Conformation Capture**

421 Chromatin conformation capture was performed as described previously described (20) with minor
422 modifications.

423

424 **Mathematical modelling**

425 The models used in this study are constructed within a framework we have previously developed and
426 experimentally validated (29,30). In addition to what is captured by previous models, our new model also
427 incorporates the dynamics of H3K36me3 and H3K27me3 at *FLC*, as observed in *ColFRI* and the
428 *COOLAIR* defective mutants.

429

430 **Acknowledgements**

431 The authors would like to thank members of the Dean lab for thoughtful inputs and Shuqin Chen for
432 excellent technical assistance. This work was funded by European Research Council Advanced Grant
433 (EPISWITCH, 833254), Wellcome Trust (210654/Z/18/Z), and a Royal Society Professorship
434 (RP\R1\180002) to CD, and BBSRC Institute Strategic Programmes (BB/J004588/1 and BB/P013511/1)
435 and EPSRC/BBSRC Physics of Life grant (EP/T00214X/1) to MH and CD.

436

437 **References**

- 438 1. Z. Xu, *et al.*, Antisense expression increases gene expression variability and locus interdependency.
439 *Mol. Syst. Biol.* **7**, 468 (2011).
- 440 2. T. Brown, *et al.*, Antisense transcription-dependent chromatin signature modulates sense transcript
441 dynamics. *Mol. Syst. Biol.* **14**, e8007 (2018).
- 442 3. C. C. Sheldon, D. T. Rouse, E. J. Finnegan, W. J. Peacock, E. S. Dennis, The molecular basis of
443 vernalization: the central role of *FLOWERING LOCUS C (FLC)*. *Proc. Natl. Acad. Sci. U. S. A.* **97**,
444 3753–3758 (2000).
- 445 4. S. D. Michaels, R. M. Amasino, *FLOWERING LOCUS C* encodes a novel MADS domain protein
446 that acts as a repressor of flowering. *Plant Cell* **11**, 949–956 (1999).
- 447 5. S. Swiezewski, F. Liu, A. Magusin, C. Dean, Cold-induced silencing by long antisense transcripts of
448 an Arabidopsis Polycomb target. *Nature* **462**, 799–802 (2009).
- 449 6. H. Yang, *et al.*, Distinct phases of Polycomb silencing to hold epigenetic memory of cold in
450 Arabidopsis. *Science* **357**, 1142–1145 (2017).
- 451 7. E. J. Finnegan, E. S. Dennis, Vernalization-induced trimethylation of histone H3 lysine 27 at *FLC* is
452 not maintained in mitotically quiescent cells. *Curr. Biol.* **17**, 1978–1983 (2007).
- 453 8. S. Berry, M. Hartley, T. S. G. Olsson, C. Dean, M. Howard, Local chromatin environment of a
454 Polycomb target gene instructs its own epigenetic inheritance. *Elife* **4** (2015).
- 455 9. S. Sung, R. M. Amasino, Vernalization in Arabidopsis thaliana is mediated by the PHD finger
456 protein VIN3. *Nature* **427**, 159–164 (2004).

- 457 10. M. Fiedler, *et al.*, Head-to-tail polymerization by VEL proteins underpins cold-induced Polycomb
458 silencing in flowering control. *Cell Rep.* **41**, 111607 (2022).
- 459 11. S. Rosa, S. Duncan, C. Dean, Mutually exclusive sense–antisense transcription at *FLC* facilitates
460 environmentally induced gene repression. *Nat. Commun.* **7**, 1–7 (2016).
- 461 12. C. A. Helliwell, M. Robertson, E. J. Finnegan, D. M. Buzas, E. S. Dennis, Vernalization-repression
462 of Arabidopsis *FLC* requires promoter sequences but not antisense transcripts. *PLoS One* **6**, e21513
463 (2011).
- 464 13. M. Jeon, *et al.*, Vernalization-triggered expression of the antisense transcript COOLAIR is mediated
465 by *CBF* genes. *Elife* **12** (2023).
- 466 14. T. Csorba, J. I. Questa, Q. Sun, C. Dean, Antisense COOLAIR mediates the coordinated switching
467 of chromatin states at *FLC* during vernalization. *Proc. Natl. Acad. Sci. U. S. A.* **111**, 16160–16165
468 (2014).
- 469 15. Y. Zhao, *et al.*, Natural temperature fluctuations promote COOLAIR regulation of *FLC*. *Genes Dev.*
470 **35**, 888–898 (2021).
- 471 16. J. Hepworth, *et al.*, Natural variation in autumn expression is the major adaptive determinant
472 distinguishing Arabidopsis *FLC* haplotypes. *Elife* **9** (2020).
- 473 17. J. A. Martens, L. Laprade, F. Winston, Intergenic transcription is required to repress the
474 *Saccharomyces cerevisiae* *SER3* gene. *Nature* **429**, 571–574 (2004).
- 475 18. T. Nguyen, *et al.*, Transcription mediated insulation and interference direct gene cluster expression
476 switches. *Elife* **3**, e03635 (2014).
- 477 19. Y. Zhao, R. L. Antoniou-Kourouniotti, G. Calder, C. Dean, M. Howard, Temperature-dependent
478 growth contributes to long-term cold sensing. *Nature* **583**, 825–829 (2020).
- 479 20. P. Crevillén, C. Sonmez, Z. Wu, C. Dean, A gene loop containing the floral repressor *FLC* is
480 disrupted in the early phase of vernalization. *EMBO J.* **32**, 140–148 (2013).
- 481 21. Z. Li, D. Jiang, Y. He, FRIGIDA establishes a local chromosomal environment for *FLOWERING*
482 *LOCUS C* mRNA production. *Nat Plants* **4**, 836–846 (2018).
- 483 22. X. Luo, T. Chen, X. Zeng, D. He, Y. He, Feedback regulation of *FLC* by *FLOWERING LOCUS T*
484 (*FT*) and *FD* through a 5' *FLC* promoter region in Arabidopsis. *Mol. Plant* **12**, 285–288 (2019).
- 485 23. X. Fang, *et al.*, The 3' processing of antisense RNAs physically links to chromatin-based
486 transcriptional control. *Proceedings of the National Academy of Sciences* **117**, 15316–15321 (2020).
- 487 24. Y. Tian, *et al.*, PRC2 recruitment and H3K27me3 deposition at *FLC* require FCA binding of
488 COOLAIR. *Sci. Adv.* **5**, eaau7246 (2019).
- 489 25. R. L. Antoniou-Kourouniotti, *et al.*, Integrating analog and digital modes of gene expression at
490 Arabidopsis *FLC*. *Elife* **12** (2023).
- 491 26. S. Oya, M. Takahashi, K. Takashima, T. Kakutani, S. Inagaki, Transcription-coupled and
492 epigenome-encoded mechanisms direct H3K4 methylation. *Nat. Commun.* **13**, 4521 (2022).

- 493 27. D. C. Zhu Pan, Reply to: Cold induction of nuclear FRIGIDA condensation in Arabidopsis. *Nature*
494 (2023).
- 495 28. H. Nishio, *et al.*, Repressive chromatin modification underpins the long-term expression trend of a
496 perennial flowering gene in nature. *Nat. Commun.* **11**, 2065 (2020).
- 497 29. R. L. Antoniou-Kourouniotti, *et al.*, Temperature Sensing Is Distributed throughout the Regulatory
498 Network that Controls *FLC* Epigenetic Silencing in Vernalization. *Cell Syst* **7**, 643-655.e9 (2018).
- 499 30. J. I. Qüesta, *et al.*, Noncoding SNPs influence a distinct phase of Polycomb silencing to destabilize
500 long-term epigenetic memory at Arabidopsis *FLC*. *Genes Dev.* **34**, 446–461 (2020).
- 501 31. R. Ietswaart, S. Rosa, Z. Wu, C. Dean, M. Howard, Cell-Size-Dependent Transcription of *FLC* and
502 Its Antisense Long Non-coding RNA COOLAIR Explain Cell-to-Cell Expression Variation. *Cell*
503 *Syst* **4**, 622-635.e9 (2017).
- 504 32. P. Kindgren, R. Ard, M. Ivanov, S. Marquardt, Transcriptional read-through of the long non-coding
505 RNA SVALKKA governs plant cold acclimation. *Nat. Commun.* **9**, 4561 (2018).
- 506 33. N. Fong, T. Saldi, R. M. Sheridan, M. A. Cortazar, D. L. Bentley, RNA Pol II Dynamics Modulate
507 Co-transcriptional Chromatin Modification, CTD Phosphorylation, and Transcriptional Direction.
508 *Mol. Cell* **66**, 546-557.e3 (2017).
- 509 34. H. Yang, M. Howard, C. Dean, Antagonistic roles for H3K36me3 and H3K27me3 in the cold-
510 induced epigenetic switch at Arabidopsis *FLC*. *Curr. Biol.* **24**, 1793–1797 (2014).
- 511 35. B. M. Zee, *et al.*, In vivo residue-specific histone methylation dynamics. *J. Biol. Chem.* **285**, 3341–
512 3350 (2010).
- 513 36. A. R. Gendall, Y. Y. Levy, A. Wilson, C. Dean, The *VERNALIZATION 2* gene mediates the
514 epigenetic regulation of vernalization in Arabidopsis. *Cell* **107**, 525–535 (2001).
- 515 37. R. Bastow, *et al.*, Vernalization requires epigenetic silencing of *FLC* by histone methylation. *Nature*
516 **427**, 164–167 (2004).
- 517 38. C. Xu, *et al.*, R-loop resolution promotes co-transcriptional chromatin silencing. *Nat. Commun.* **12**,
518 1790 (2021).
- 519 39. D.-H. Kim, S. Sung, Vernalization-Triggered Intragenic Chromatin Loop Formation by Long
520 Noncoding RNAs. *Dev. Cell* **40**, 302-312.e4 (2017).
- 521 40. J. B. Heo, S. Sung, Vernalization-mediated epigenetic silencing by a long intronic noncoding RNA.
522 *Science* **331**, 76–79 (2011).
- 523 41. P. Zhu, M. Schon, J. Questa, M. Nodine, C. Dean, Causal role of a promoter polymorphism in
524 natural variation of the Arabidopsis floral repressor gene *FLC*. *Curr. Biol.* (2023).
- 525 42. R. Ye, *et al.*, Glucose-driven TOR–FIE–PRC2 signalling controls plant development. *Nature* **609**,
526 986–993 (2022).
- 527 43. D. J. Gibbs, *et al.*, Oxygen-dependent proteolysis regulates the stability of angiosperm polycomb
528 repressive complex 2 subunit *VERNALIZATION 2*. *Nat. Commun.* **9**, 5438 (2018).

- 529 44. U. Amara, J. Hu, J. Cai, H. Kang, FLK is an mRNA m6A reader that regulates floral transition by
530 modulating the stability and splicing of *FLC* in Arabidopsis. *Mol. Plant* **16**, 919–929 (2023).
- 531 45. B. Sun, *et al.*, FIONA1-mediated methylation of the 3'UTR of *FLC* affects *FLC* transcript levels and
532 flowering in Arabidopsis. *PLoS Genet.* **18**, e1010386 (2022).
- 533 46. J. P. Uhler, C. Hertel, J. Q. Svejstrup, A role for noncoding transcription in activation of the yeast
534 PHO5 gene. *Proc. Natl. Acad. Sci. U. S. A.* **104**, 8011–8016 (2007).
- 535 47. F. Bardou, *et al.*, Long noncoding RNA modulates alternative splicing regulators in Arabidopsis.
536 *Dev. Cell* **30**, 166–176 (2014).
- 537 48. U. Chorostecki, N. G. Bologna, F. Ariel, The plant noncoding transcriptome: a versatile
538 environmental sensor. *EMBO J.*, e114400 (2023).
- 539 49. E. Franco-Echevarría, *et al.*, Distinct accessory roles of Arabidopsis VEL proteins in Polycomb
540 silencing. *Genes. Dev.* **37**, 801–817 (2023).

541

542 **Figures**

543

544 **Figure 1. *ntl8-D3* mimics cold exposure, except for the accumulation of H3K27me3.**

545 (A) Expression of total *COOLAIR* and *VIN3* in *ntl8-D3 FRI* and in *ColFRI* in non-vernalized conditions
546 (NV). Data are presented as the mean \pm s.e.m. Each open circle represents a biological replicate. (B-D)
547 Enrichment of (B) H3K36me3, (C) H3K27me3, and (D) H2Aub across *FLC* measured by ChIP in wild-
548 type *ColFRI* and *ntl8-D3* at NV conditions. H3K36me3 data are shown relative to H3, and actin.
549 H3K27me3 data are shown relative to H3, and STM. H2Aub data are shown relative to H3. Error bars
550 represent s.e.m ($n \geq 3$ biological replicates). (E) VIN3-eGFP ChIP-qPCR enrichment at *FLC* at NV. Data
551 are shown as the percentage input. Non-transgenic *ColFRI* plants were used as a negative control sample.
552 Error bars represent s.e.m ($n = 3$ biological replicates). (F) Enrichment of H3K27me2 across *FLC*
553 measured by ChIP in wild-type *ColFRI* and *ntl8-D3* at NV conditions. Data are expressed relative to H3.
554 Error bars represent s.e.m ($n = 3$ biological replicates). (G) Quantitative 3C-qPCR over the *FLC* locus in
555 10-day-old *ColFRI* and *ntl8-D3 FRI* seedlings. A schematic representation of the *FLC* locus is shown
556 above. BamHI and BglII restriction sites are indicated with dotted lines, and the respective regions are
557 numbered with Roman numerals. Red arrows indicate the location of the primers used for 3C-qPCR. The
558 region around the *FLC* transcription start site was used as the anchor region in the 3C analysis. The data
559 below shows the relative interaction frequencies (RIF).

560

561 **Figure 2. Cold-induced chromatin and RNA dynamics in *COOLAIR* defective lines.**

562 (A-B) Enrichment of H3K27me3 (A) and H3K36me3 (B) across *FLC* measured by ChIP in wild-type
563 *ColFRI* and the three defective *COOLAIR* lines, *TEX1*, *TEX2*, and *FLC_{ΔCOOLAIRs}* before, during, and after
564 vernalization. Data are expressed relative to H3 and *STM*. Error bars represent s.e.m. (n = 3 biological
565 replicates). (C-D) Average levels of H3K27me3 (C) and H3K36me3 (D) in the nucleation region during
566 vernalization. The averages were calculated by averaging the ChIP enrichment over three primers in the
567 *FLC* nucleation region during vernalization in *ColFRI* and each of the defective *COOLAIR* lines. (E-F)
568 *FLC* expression during a vernalization time course in *ColFRI* and the three defective *COOLAIR* lines,
569 Unspliced (E) and spliced RNA (F), was measured and is shown relative to *UBC* and *NV* levels. Error
570 bars represent s.e.m. (n = 3 biological replicates).

571

572 **Figure 3. Fluctuating cold and mathematical modelling of the role of *COOLAIR* in histone**
573 **modification dynamics.** (A-B) Changes in H3K36me3 (A) and H3K27me3 (B) at *FLC* after two weeks
574 of Constant Cold (CC), Fluctuating Mild (FM), or Fluctuating Strong (FS) conditions, measured by ChIP-
575 qPCR. Data are expressed relative to H3. Error bars represent s.e.m. (n = 3 biological replicates). (C-D)
576 Comparing changes in H3K36me3 at *FLC* between *ColFRI* (C) and *TEX1 flclean* (D) after two weeks of
577 FM or FS conditions, measured by ChIP-qPCR. Data are expressed relative to H3 and *STM*. Error bars
578 represent s.e.m. (n = 3 biological replicates). (E) Schematic of the mathematical model showing core
579 components: PRC2 mediated silenced states (non-nucleated, nucleated and spread) at individual *FLC*
580 alleles, antisense transcription mediated repression of *FLC* transcription, and the contribution of these
581 components to the average population level H3K36me3 coverage at the *FLC* locus.

582

583 **Figure 4. Model predictions of the impact of vernalization mutants on histone dynamics and**
584 **schematic representation of parallel pathways that repress *FLC* expression.**

585 (A-D) Mathematical model predicted levels of H3K36me3 (A,B) and H3K27me3 (C,D) over a constant
586 cold time course in a defective *COOLAIR* mutant (A,C) and the wild type, *ColFRI* (B,D). The predictions
587 are compared to the ChIP-qPCR time course data for the different genotypes presented in Fig. 2(A,B). (E)
588 Model for the parallel pathways that repress *FLC*. In the warm *FLC* forms a gene-loop conformation,
589 which mediates a high expression state of *FLC*. The high expression state is marked by high levels of
590 H3K36me3 around the *FLC* TSS. After cold exposure, the repressive pathways are activated: (1) The
591 antisense-mediated pathway leading to disruption of the gene-loop and removal of H3K36me3 from the
592 TSS of *FLC*. (2) The Polycomb pathway leading to deposition of H3K27me3 and repression of *FLC*
593 transcription. The two pathways work in parallel rather than through a linear sequence of causation to
594 give the final *FLC* expression outcome during vernalization.

595

596

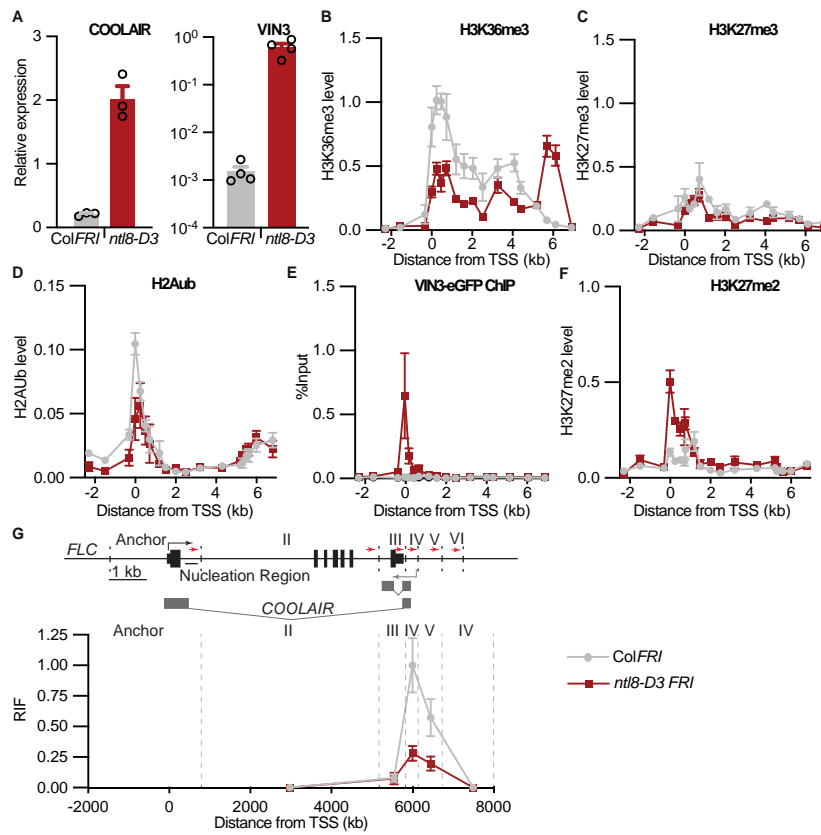
597

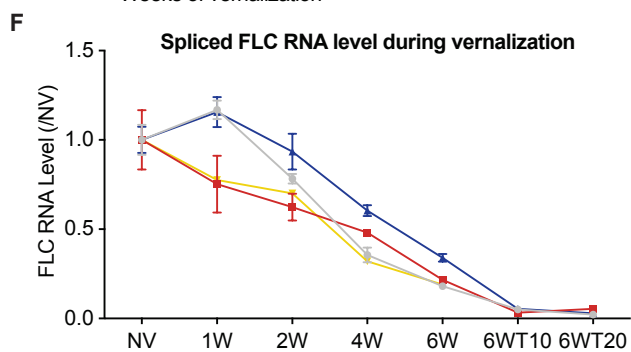
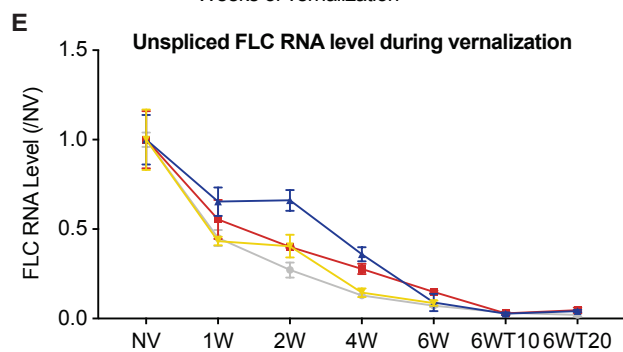
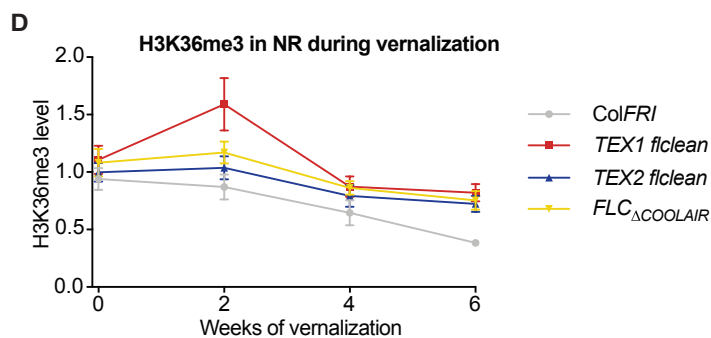
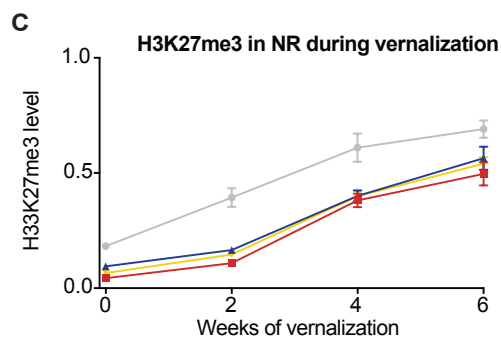
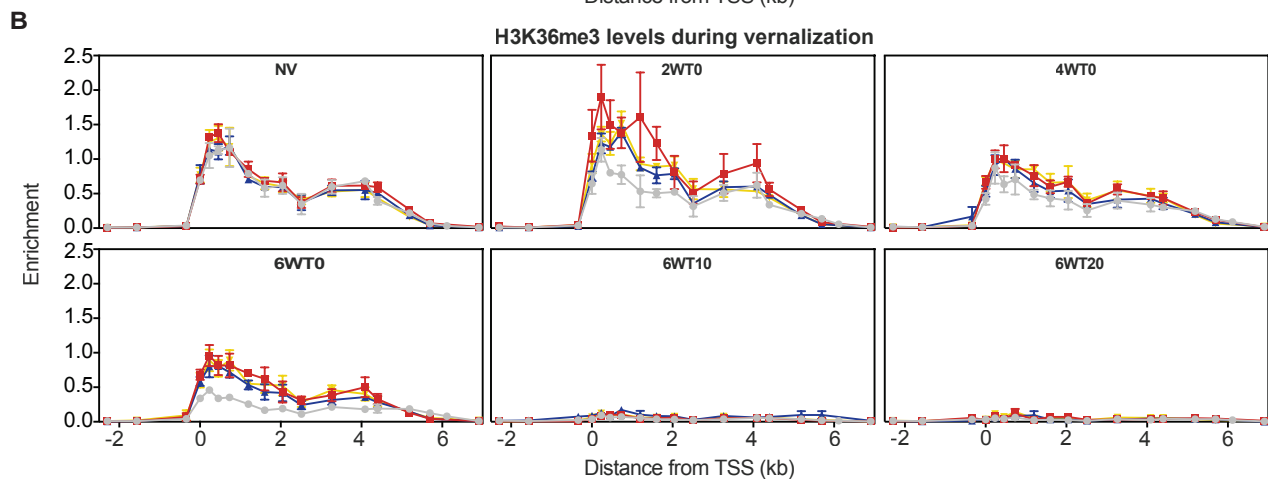
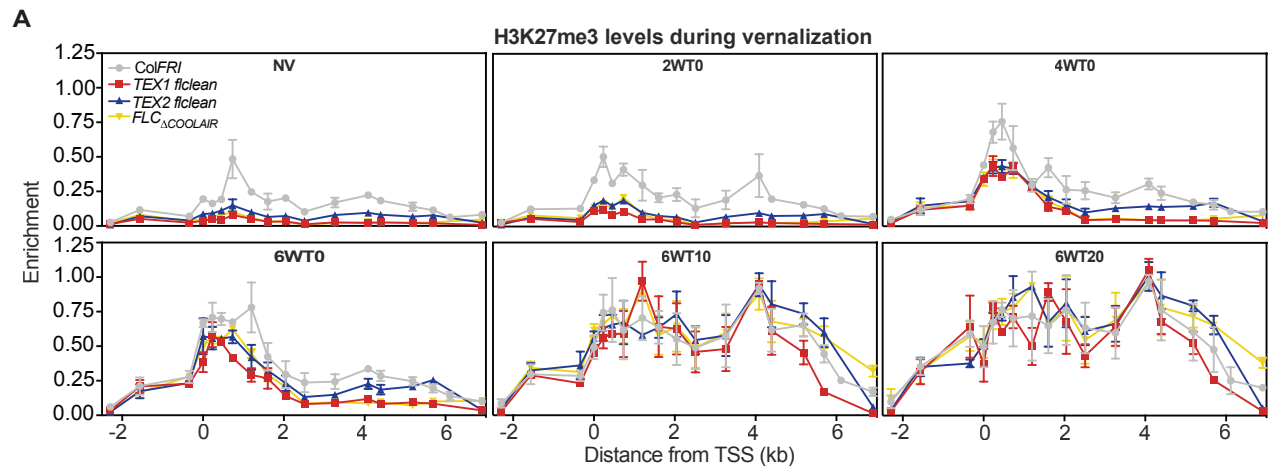
598

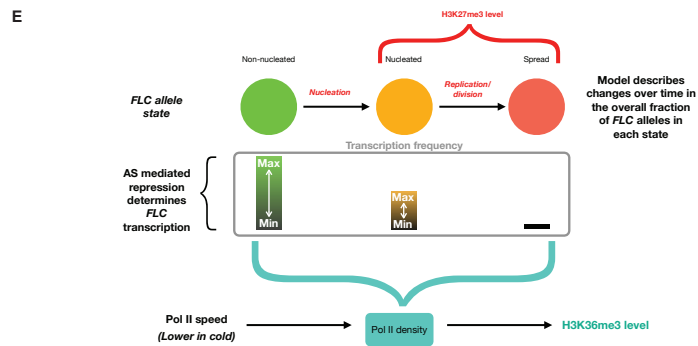
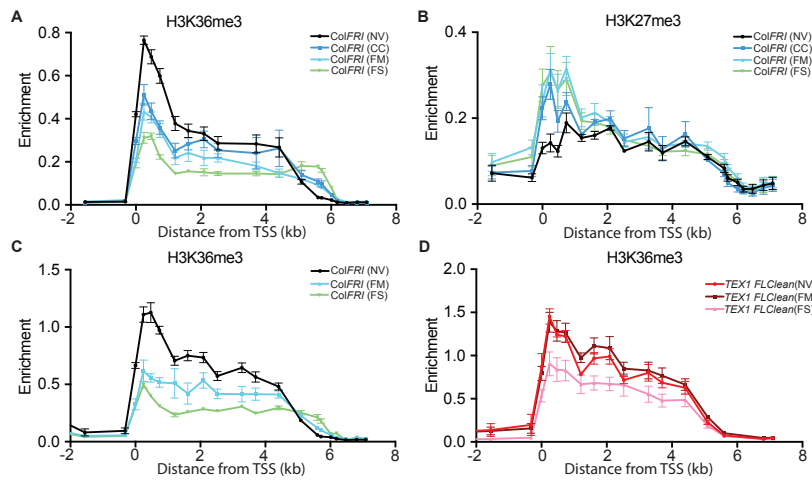
599

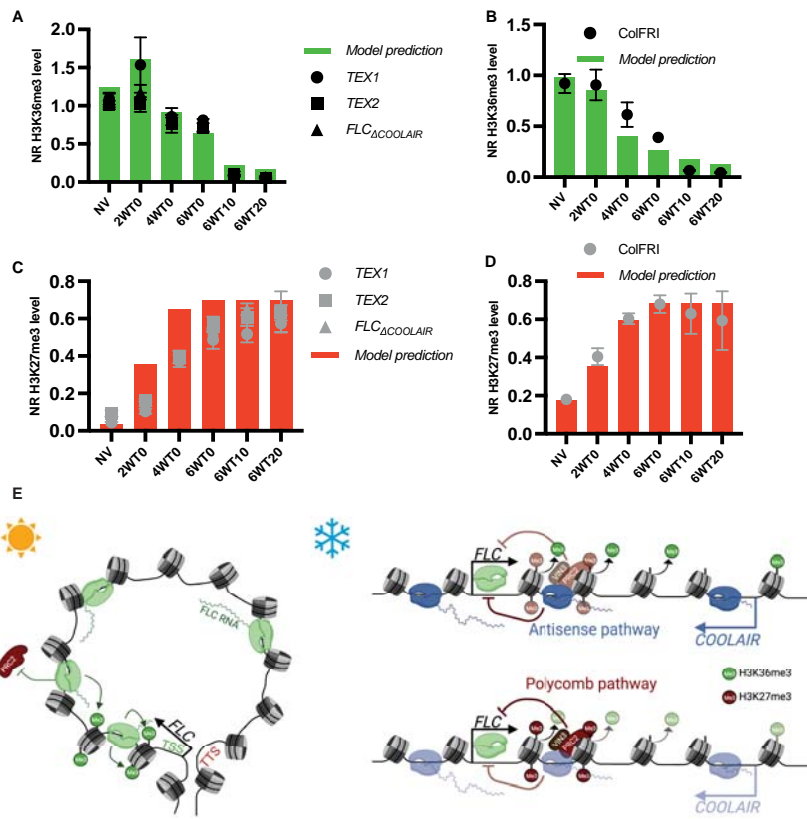
600

601











Supporting Information for
Antisense transcription and PRC2 repression function in parallel during vernalization

Mathias Nielsen[†], Govind Menon[†], Yusheng Zhao, Eduardo Mateo-Bonmati, Philip Wolff, Shaoli Zhou,
Martin Howard* & Caroline Dean*

*Corresponding authors Caroline Dean and Martin Howard

Email: caroline.dean@jic.ac.uk; martin.howard@jic.ac.uk

This PDF file includes:

Supporting text
Figures S1 to S10
Table S1 to S2
Legend for Dataset S1
SI References

SI Materials and Methods

Plant materials

All mutant and transgenic lines were in the *FRI*^{sf2} background. Mutant alleles were described previously: *ntl8-D3 FRI* (1), and *FLC_{ΔCOOLAIR}* (2). For this study, *FLC_{ΔCOOLAIR}* was introduced into Columbia with an active *FRIGIDA* allele (3). The *TEX1.0* and *TEX2.0* constructs were described previously (1, 4), and for this study, the constructs were introduced into *FLCclean* by floral dipping. *FLCclean* was created by CRISPR-CAS9. The CRISPR guide-RNA sequences were: sgRNA_1: attGAAAAGGGCAAGGAGGTGGTgttttagagctagaaatagcaag, sgRNA_3: attGGCGGAGGAGCAGCCGCAAGgttttagagctagaaatagcaag, sgRNA_2: attGGGCGGACTCACGTTAGTCAgttttagagctagaaatagcaag, sgRNA_4: attGTTGGAGCGCGTGAGGATCAgttttagagctagaaatagcaag.

Regions that map to the locus are in capital letters, mapping immediately upstream of the PAM motif (NGG). The long 3'-tail corresponds to the scaffold for Cas9 binding. Two *FLCclean* lines were created *FLCclean_13*, with sgRNA 1 and 3, and *FLCclean_24*, with sgRNA 2 and 4. The *FLCclean_24* line was used as background for floral dipping with the *TEX1.0* and *TEX2.0* constructs. The *pVRN5:VIN3-eGFP* line was generated by replacing the *VIN3* promoter sequence from the *pVIN3:VIN3-eGFP* construct described previously (5) with the promoter sequence of *VRN5*. The construct was transformed into *vin3-4 FRI* by floral dipping, and individual lines were selected. Two individual lines (#28 and #40) were used for ChIP analysis.

Growth conditions

Seeds were surface sterilized and sown on 1x Murashige and Skoog (MS) media without glucose. As *FLC* shutdown in cold is sensitive to growth, seeds for expression analysis were sown at low density. Seeds were stratified for 2–3 days at 4°C and grown for 10 days under long-day conditions (16h light, 8h dark at 20°C). For vernalization treatment, seedlings were transferred to short-day conditions (8h light, 16h darkness at constant 5°C) after 10 days pre-growth. Plants harvested 10 days after vernalization were transferred back to long-day conditions and harvested from plates. For longer post-vernalization treatment (more than 10 days), the plants were transferred to soil and grown under long-day conditions. Fluctuating cold conditions used in Fig. 3 were as described previously (1).

Expression analysis

Total RNA was extracted using the hot phenol method as described previously (6). Genomic DNA contamination was removed with TURBO DNase (Invitrogen), following the manufacturer's guidelines. cDNA was synthesized with SuperScript IV reverse transcriptase (Invitrogen). Gene-specific primers were used for reverse transcription (RT) of *COOLAIR*, *FLC*, and *VIN3*. For the RT reaction to analyse the expression of vernalization factors in SI Fig. 1, oligo(dT) primers were used. Quantitative PCR (qPCR) was performed using SYBR Green I Master (Roche) and analysed on a LightCycler 480 machine (Roche). Ct values were normalized to the geometric mean of *UBIQUITIN CARRIER PROTEIN 1 (UBC)* and *SERINE/THREONINE PROTEIN PHOSPHATASE 2 A (PP2A)*. All primers are listed in SI Appendix, Table S1.

Chromatin immunoprecipitation

Chromatin immunoprecipitation (ChIP) was performed as described in (7). ChIP was performed with antibodies: α -H3 (Abcam, ab1791), α -H3K36me3 (Abcam, ab9050), α -H3K27me3 (Abcam, ab192985), α -H3K27me2 (Upstate, 07-452), α -H2AK119ub (Cell Signaling Technology, #8240), α -H3K4me1 (Abcam, ab8895), and α -GFP (Abcam, ab290). ChIP enrichment was quantified by qPCR with primers listed in SI Appendix, Table S1. For histone, ChIP values were normalized to H3. For H3K36me3 and H3K27me3, values were further normalized to enrichment at the positive control loci *ACTIN* for H3K36me3 and *STM* for H3K27me3. Primers; *FLC* 0, *FLC* 250, and *FLC* 500 were used to calculate the average level in the nucleation region for the plots in Fig. 2 and SI Fig. 5.

Chromatin Conformation Capture

Chromatin conformation capture was performed as described previously (8, 9) with minor modifications. 1 g of 10 days old seedlings were crosslinked in 2 % formaldehyde for 20 mins. Crosslinking was stopped by the addition of 2M Glycin to a final concentration of 0.125 M and vacuum infiltrated for 7 mins. Nuclei were extracted with Honda buffer as for ChIP (7). After purification, chromatin was digested with 600 U of BamHI (NEB) and BglII (NEB) for 14-16 h, followed by 8h of ligation with T4 ligation (Promega) at 17°C. DNA was purified with Phenol:Chloroform:IAA (25:24:1) and precipitated with isopropanol. DNA was dissolved in water

and further purified using the CHIP DNA Clean & Concentration (Zymo Research) kit, following the manufacturer's protocol. The 3C library was quantified as described previously (8).

The same primers were used to analyse TEX2.0, as the NOS sequence inserted in TEX2.0 contains no additional BglII or BamHI restriction sites.

Mathematical modelling

In this study we use mathematical modelling to dissect the complex interplay of Polycomb mediated silencing and antisense mediated repression involved in *FLC* regulation in the cold. The models used in this study are constructed within a framework we have previously developed and experimentally validated. This framework describes the dynamics of transcriptional shutdown and histone modification changes at the whole-plant level during cold-induced epigenetic silencing at *FLC* (10, 11). Therefore, the assumptions used in these previous models are carried through into the models developed here. Many of these assumptions are directly based on experimentally established details, while the validity of others has been established through experimental testing of model predictions in these previous studies (10, 11). The models developed in this study use these assumptions as a starting point before we add additional features.

H3K36me3 and H3K27me3 dynamics in *COOLAIR* defective mutants

Our previously developed (and experimentally validated) models successfully captured the behaviour of H3K27me3 at *FLC* in cold and post-cold conditions observed in *ColFRI*, nucleation mutants, spreading mutants, as well as reactivation in a natural variant of *FLC*. These models also captured some, although not all, aspects of H3K36me3 dynamics. However, these models did not capture the role of antisense mediated regulation. Here, we start with the existing modelling framework, and attempt to build a model that, in addition to what is captured by previous models, can also properly incorporate the dynamics of H3K36me3 and H3K27me3 at *FLC* as observed in *ColFRI* and the *COOLAIR* defective mutants. To do this we focus on only those trends which are consistent across the three different *COOLAIR* defective mutants. These features are as follows (Fig. 2):

1. Similar dynamics of H3K27me3 nucleation and spreading in *ColFRI* and *COOLAIR* defective mutants, with a significant difference in starting (NV) levels.
 - H3K27me3 nucleation is not slower in *COOLAIR* defective mutants.
 - H3K27me3 levels at 6WT0 are similar in *ColFRI* and *COOLAIR* defective mutants.
 - H3K27me3 spreading is similar in *ColFRI* and *COOLAIR* defective mutants.

2. Significant differences in H3K36me3 dynamics of the *COOLAIR* defective mutants during the cold.
 - H3K36me3 increases across the locus (relative to NV) in the *COOLAIR* defective mutants in the first two weeks of cold, while *ColFRI* does not show this trend.
 - The overall reduction in H3K36me3 levels over six weeks of cold is clearly weakened in the *COOLAIR* defective mutants, so that they exhibit significantly higher levels of this modification across the locus at 6WT0.
 - Consistent with H3K36me3 changes and the association of this modification with transcription, *FLC* unspliced also reduces more slowly in the *COOLAIR* defective mutants.
3. Similar behaviour of H3K36me3 in *COOLAIR* defective mutants and in *ColFRI* during post-cold growth.
 - A clear reduction of H3K36me3 levels is observed between 6WT0 and 6WT10/T20, in both *COOLAIR* defective mutants and *ColFRI*.
 - Consistent with H3K36me3 reduction, and the association of this modification with transcription, *FLC* transcriptional output also reduces further in the post-cold.

Building a model to capture the differences in H3K36me3 dynamics

The behaviour of H3K27me3 in the *COOLAIR* defective mutants (described above) can be captured by previous models, since the behaviour is similar to *ColFRI*, except for the difference in NV levels. However, these models cannot capture the H3K36me3 behaviour, which shows significant differences in the *COOLAIR* defective mutants. This is because: (i) these models do not explicitly include a regulatory role for antisense transcription, and (ii) these models treat H3K36me3 and H3K27me3 as being exclusively present in different states of the *FLC* locus (H3K36me3 only in a high transcriptional state, and H3K27me3 only in a nucleated or spread state).

Capturing *FLC* states at the whole plant level

The existing modelling framework describes *FLC* locus states in a population of cells representing the whole plant. This population is made up of dividing and non-dividing cells (10,11). One of the core assumptions of these models is that the *FLC* locus can undergo nucleation of H3K27me3 in both dividing (meristematic tissue) and non-dividing cells. The validity of this assumption is supported by both direct and indirect experimental evidence: (i) for dividing cells, measurements of *FLC* epigenetic silencing by Polycomb in root meristematic cells via fluorescent imaging of *FLC*-Venus in plants defective for spreading of H3K27me3 (12); (ii) for non-dividing cells, the direct measurement of H3K27me3 nucleation by ChIP in mature leaves during vernalization in *ColFRI* (13); (iii) for non-dividing cells, the indirect evidence from all of our own ChIP time course datasets for H3K27me3: If only copies in dividing cells were capable of

nucleation, the repeated division of these nucleated copies during rapid post-cold growth would cause a significant increase in population-level nucleation region H3K27me3. The fact that no such increase is observed by ChIP during post-cold growth indicates that *FLC* copies in both dividing and non-dividing cells can nucleate. This continues to be a core assumption in the models built here. As discussed in the main text, our data indicates that the antisense mediated repression and the PRC2/H3K27me3 mediated silencing function in parallel at *FLC*. This paradigm of two parallel pathways is therefore also central to the models developed here.

Possible models with different behaviour in subpopulations of cells

With the previously observed mutual exclusivity of H3K27me3 and H3K36me3 at *FLC* during vernalization (14), as well as other evidence for the mutual exclusivity of these modifications (15), it is tempting to consider models where apparent disruption of this mutual exclusivity in *COOLAIR* defective mutants arises from different subpopulations of *FLC* copies ending up in different states. While some tissue specific behaviour cannot be ruled out, here we examine two simple models with different behaviour between subpopulations and demonstrate that such subpopulation specific behaviour by itself is insufficient to capture the observed trends.

Model 1: A simple approach to explain the difference in H3K36me3 dynamics during the cold between *ColFRI* and the *COOLAIR* defective lines, using the existing models, would be to introduce a subpopulation of cells *only* in the *COOLAIR* defective mutants, in which H3K27me3 does not nucleate at *FLC* in the cold. These *FLC* copies would remain in an active transcriptional state, thus producing a higher level of H3K36me3 during the cold in the *COOLAIR* defective lines. However, the presence of such a non-nucleating subpopulation would be expected to produce a clear reduction of nucleation region H3K27me3 levels (compared to *ColFRI*) during the cold. Since this is not observed, particularly at 6WT0, we reject this model.

Model 2: A more sophisticated model to explain the difference in H3K36me3 dynamics in the cold is one where we again have a subpopulation of non-nucleating cells, but this subpopulation is common to both *ColFRI* and the *COOLAIR* defective mutants. This subpopulation has to include roughly the same proportion of dividing cells as the rest of the population (otherwise this model would produce a post-cold increase in nucleation region H3K27me3, which as discussed above, is inconsistent with all our data). The existence of such a subpopulation would allow H3K27me3 dynamics to be unchanged between these genotypes. The higher H3K36me3 in the *COOLAIR* defective mutants could then be explained by antisense mediated repression having a role specifically in the non-nucleating subpopulation. However, since the

non-nucleating population includes dividing cells, their active *FLC* states (and hence high H3K36me3 levels) would be maintained and propagated during post cold growth. Therefore, without invoking additional, unknown mechanisms for H3K36me3 removal in this subpopulation of cells, even this model cannot explain the post cold reduction in H3K36me3 leading to essentially the same levels in *ColFRI* and the *COOLAIR* defective mutants by 6WT10.

Thus, we are led to construct a model where H3K27me3 and H3K36me3 can co-exist at the same *FLC* copy, and where antisense transcription mediated repression can modulate sense transcription associated H3K36me3 levels. We note that the coexistence of the two marks could potentially involve coexistence on the same H3 tail - H3K27me3 accumulation at *FLC* during cold is mediated by a VRN2-PRC2 complex, whose activity has been shown to be insensitive to the presence of H3K36me3 on a substrate H3 tail (15). To capture the rapid response of this pathway observed under fluctuating temperatures (1), our model also includes a fast timescale response capability for the antisense mediated repression pathway. The mathematical model is detailed below.

Model features

Chromatin states at *FLC* copies: The model allows each copy to be in one of three states: an active transcriptional state (no H3K27me3 nucleation), an H3K27me3 nucleated state, and an H3K27me3 spread state. Importantly, the model also allows H3K36me3 to be present at the locus in *all of these states*, at a level that is determined by the transcriptional activity possible in each state rather than direct mutual exclusivity with H3K27me3. This means that the *FLC* copies in the active transcriptional state (no H3K27me3 nucleation) make the highest contribution to population level H3K36me3 levels; copies in the H3K27me3 nucleated state have lower transcriptional activity and hence make an intermediate contribution to population level H3K36me3; copies in the H3K27me3 spread state have the lowest transcriptional activity and hence make the lowest contribution to population level H3K36me3. We note that the above features replace the assumptions used in previous models (10,11) :

- (1) Allowing H3K36me3 to be present in all states at a level determined by transcriptional activity replaces the previous assumption that this modification is only present in a high transcriptional state of *FLC*.
- (2) Having only three states of the locus – active, H3K27me3 nucleated, and H3K27me3 spread – replaces the assumption that there is a distinct, “inactive” state of the locus with neither H3K36me3 nor H3K27me3 accumulation, which is set up by a “VIN3 independent” pathway.

The new assumptions allow the model to capture transcriptional downregulation and H3K36me3 levels in parallel to H3K27me3 mediated changes of transcriptional state, and thus emphasises the paradigm that emerges from our data – that of parallel pathways (antisense transcription mediated and PRC2 mediated) converging to regulate *FLC* expression.

Dividing and Non-dividing loci: The total number of dividing copies is fixed. We use a simplified division model (11), where each division produces one dividing copy and a fixed number of non-dividing copies.

Nucleation and Spreading:

- Transitions from an active to a nucleated state are allowed only in the cold, with the probability of nucleation dictated by the VIN3 protein concentration calculated from the LSCD model of VIN3 dynamics (10) – a predictive model of VIN3 expression that captures the effect of multiple thermosensory inputs operating at different timescales.
- The transition from a nucleated to a spread state occurs during replication/division, consistent with the dependence of spreading on an active cell cycle that we have previously shown (12).
- Replication/division causes a transition from a nucleated to a spread state: each division of a nucleated copy produces one dividing, spread copy and a fixed number of non-dividing, spread copies.
- The spread state is assumed to be stable – the model does not allow reactivation from the spread state.
- Except in simulations of the spreading mutant, we assume no loss of nucleation at nucleated, dividing copies.

Division rate and pre-growth duration

- The growth rate is assumed to undergo a step change in the cold (5°C) conditions - reduced by a factor of 40 relative to warm (22°C) conditions (11).
- The step change of growth rate is assumed to be the same in constant cold and fluctuating temperature conditions.
- The pre-growth duration is fixed at 10 days (11).

Sense transcriptional activity (initiation rate): Antisense mediated regulation of sense transcription (initiation rate) is assumed to be possible in the active and nucleated states. The highest level of transcriptional activity in the nucleated state is assumed to be 0.3 of the highest level in the active state. Based on our data, which shows that cold induced H3K27me3 nucleation and post-cold H3K27me3

spreading are not disrupted in the *COOLAIR* defective mutants, we assume that nucleation and spreading of H3K27me3 (i.e., the rates of transition to these states) are unaffected by the absence of the antisense mediated repression.

Sense transcriptional activity (PolII speed): The increase in H3K36me3 between NV and 2WT0 observed in the *COOLAIR* defective mutants cannot be captured by only having co-transcriptional addition of this modification – there is a general trend towards reduction rather than an increase in sense transcriptional activity between these timepoints (as measured by *FLC* unspliced and spliced transcript levels). Therefore, to capture this increase in H3K36me3, we introduce a reduction in the speed of RNA PolII in the nucleation region in the cold: it is assumed to undergo a step change drop to 0.6 of its NV value in the cold and also recovers post-cold. Such a reduction in Pol II speed in the nucleation region allows the Pol II dwell time to increase between the NV and 2WT0 timepoints, even with a reduction in transcriptional activity (initiation rate) between these timepoints. We assume that the same reduction in PolII speed in the nucleation region also occurs under the fluctuating temperature conditions.

Antisense mediated (nucleation independent) repression pathway: A nucleation independent repression pathway performs analogue control of the sense transcription level in active and nucleated states. The functioning of this pathway is assumed to rely on antisense (AS) transcription (i.e., this pathway is not functional in the *COOLAIR* defective mutants).

Slow timescale component: Under cold conditions, both constant and fluctuating cold, repression by the AS pathway is assumed to increase slowly in the cold and decrease quickly upon return to warm, consistent with NTL8 dynamics (16). The repression is modelled as a slow reduction in the sense transcription initiation rate in the cold, and a rapid recovery in the initiation rate in the post-cold. This is captured by a multiplicative factor set to vary between 1 and 0.5 with an exponential decay over time in cold and a faster exponential recovery over time in the warm (see model implementation below). This is consistent with our previous model-predicted NTL8 accumulation dynamics determined by slower growth in the cold (16), and rapid NTL8 reduction during post-cold growth, as well as the measured slow build-up of *FLC* antisense transcripts in constant cold measured by qPCR (17) This is also consistent with the analysis of the VIN3 independent pathway in (10) – the dynamics of this pathway was predicted to be temperature dependent, causing slow *FLC* reduction in the cold, but allowing rapid increase in the post cold in the absence of VIN3 dependent H3K27me3 nucleation. The reduction of the transcriptional initiation rate (caused by the AS pathway) is assumed to have the same dynamics at active (non-nucleated) and nucleated copies.

The transcriptional initiation recovery timescale in the post-cold is also assumed to be the same at non-nucleated and nucleated copies.

Fast timescale component: To capture the rapid response of the antisense mediated repression under fluctuating temperature conditions, we assume that low temperatures cause a large reduction in the sense transcription initiation rate (due to strong upregulation of antisense transcription). While freezing temperatures are seen to have the strongest effect on upregulating antisense transcription, we note that in our experimental data, both mild and strong fluctuating conditions cause significant downregulation of *FLC* sense transcription, with the reduction of both *FLC* mRNA and H3K36me3 being largest in FS conditions and intermediate in FM conditions. To capture these effects in both FM and FS conditions, we assume a simple step change in the antisense mediated repression. This is represented by the multiplicative factor defined above undergoing a step reduction to a value of 0.05 whenever the temperature falls below 4°C. Above this temperature, this factor takes a slow, exponentially decaying value (as a function of time) as described above (see Table S1 for definition).

Thus, under fluctuating temperature conditions we assume that, in addition to the large step changes to the multiplicative factor, a slow timescale reduction in this factor also occurs. Not including a slow timescale reduction under fluctuating conditions would cause the model to fail in capturing the observed changes to H3K36me3 and *FLC* mRNA under FM and FS conditions. Note that the reduction in Pol II speed in the nucleation region assumed for constant cold is also assumed to occur under FM and FS conditions. In the absence of this assumption – i.e., if the PolII speed is assumed to change only in constant cold conditions – the model would predict even larger changes in H3K36me3 under FM and FS conditions relative to NV.

We note that the above set of assumptions describing the antisense mediated pathway replaces population level H3K36me3 in the simpler description of a “VIN3 independent” pathway used in our previous models (10,11).

H3K27me3 levels: The contribution to H3K27me3 levels from an individual *FLC* locus depends on the state of the locus: low in the nucleation region (NR) and non-nucleation region (body) for active copies, high in the NR and low in the body for nucleated copies, high in the NR and body for spread copies.

H3K36me3 levels in the NR depend on Pol II density: For simplicity, the model describes the population level average H3K36me3 levels in the *FLC* nucleation region, but we note that the levels of this

modification across the gene body follow the trends in the nucleation region in all our data (Fig. 2B, (12,14)), with the only exception being the 3' end of the locus, where H3K36me3 levels reflect the level of antisense transcription (increasing during the cold (Fig. 3A,C), (14) and high in ntl8-D3 (Fig. 1B)). H3K36me3 is represented as a dynamical variable in the model, and based on the above evidence, the rate of addition of H3K36me3 is assumed to be proportional to the Pol II density. This is consistent with co-transcriptional addition of this modification (18), as well as longer Pol II dwell time at a given location allowing a greater window of opportunity for adding this modification (19). The Pol II density is determined by the ratio of initiation rate to PolIII speed in the nucleation region. As described above, the initiation rate is determined by two factors - the H3K27me3 state and the antisense mediated repression pathway - while the PolIII speed undergoes a step change in cold conditions. We also assume a constant turnover rate of H3K36me3 - the value of the rate constant is assumed to be 1.21 day^{-1} , consistent with the half-life of H3K36me2 (0.571 day) estimated in (20), since no data was available for H3K36me3.

FLC mRNA level: The model describes the population level average *FLC* mRNA level as a dynamical variable, whose production is determined by the sense transcription initiation rates of the *FLC* copies in different states. As described above, these initiation rates are also determined by the antisense mediated repression. We fix a turnover rate for *FLC* mRNA consistent with a half-life of 6 hr as estimated in (21).

Fluctuating temperature input to the model: The temperature profiles used to simulate FM and FS conditions are shown in Table S2. We note that in the model, based on the above assumptions, this dynamic temperature input is affecting two components – the antisense mediated repression (as described above) and the LSCD model of VIN3 dynamics (thus determining the nucleation rate) (10). Other temperature dependent rates – Pol II elongation and growth – are assumed to undergo a step change in the cold, so they are not affected by other dynamics of the temperature input.

Summary of changes from previous models

Feature	Previous models	Current model
<i>FLC</i> sense transcriptional downregulation	Captured by transition between an active (high) transcription state and an inactive state, controlled by a slow, 'VIN3 independent' pathway.	Captured by an antisense mediated repression that can modulate sense transcription in both an active transcription state and a nucleated state. This repression increases slowly in

		constant cold but can respond to temperature fluctuations on a fast timescale.
<i>FLC</i> states	Five possible states: High transcription, Inactive, Nucleated, Spread, and Perpetuated.	Three possible states: Non-nucleated active state, Nucleated state, and spread state. The perpetuated state not included since this state is not expected to play a major role in the phases of silencing examined in this study. This state can be incorporated into the current model for studying aspects such as post-cold <i>FLC</i> reactivation.
Nucleation	Transition to nucleated state partly relies on transcriptional downregulation (i.e., prior transition to inactive state).	Transition to nucleated state does not rely on antisense mediated transcriptional repression.
H3K36me3 contribution from nucleated and spread states	Assumes no contribution to overall H3K36me3 level from either nucleated or spread/perpetuated states.	Assumes a contribution to overall H3K36me3 from all states, at a level determined by the amount of transcription (therefore determined by the antisense mediated repression).
Link between H3K36me3 and RNA Pol II speed	Not captured in previous models.	Rate of addition of H3K36me3 is assumed to be inversely proportional to the PolII speed in the nucleation region, consistent with a model of co-transcriptional H3K36 methylation, dependent on Pol II dwell time. The speed is

		assumed to undergo a step reduction in the cold.
--	--	--------------------------------------------------

Model implementation

Following the same approach as for our previous models (10,11), an ODE (Ordinary Differential Equation) model is constructed using the above assumptions. The model equations are shown below. The model is simulated using the ode15s solver in Matlab version 2017a.

Model Variables:

$f_{a,d}$ (fraction of active, dividing copies)

$f_{n,d}$ (fraction of nucleated, dividing copies)

$f_{s,d}$ (fraction of spread, dividing copies)

$f_{a,nd}$ (ratio of active, non-dividing copies to total number of dividing copies)

$f_{n,nd}$ (ratio of nucleated, non-dividing copies to total number of dividing copies)

$f_{s,nd}$ (ratio of spread, non-dividing copies to total number of dividing copies)

The dynamics are such that $f_{a,d} + f_{n,d} + f_{s,d} = 1$ at all timepoints.

Basic Model (representing ColFRD):

$$\begin{aligned}\frac{df_{a,d}}{dt} &= -k_s f_{a,d} \\ \frac{df_{n,d}}{dt} &= k_s f_{a,d} - g(T) f_{n,d} \\ \frac{df_{s,d}}{dt} &= g(T) f_{n,d} \\ \frac{df_{a,nd}}{dt} &= d_n g(T) f_{a,d} - k_s f_{a,nd}\end{aligned}$$

$$\frac{df_{n,nd}}{dt} = k_s f_{a,nd}$$

$$\frac{df_{s,nd}}{dt} = d_n g(T) f_{n,d} + d_n g(T) f_{s,d}$$

$$\frac{d[H3K36me3]}{dt} = k_{K36me3}^d (G_{K36} (F_a, F_n, F_s) - [H3K36me3])$$

$$\frac{d [FLC]}{dt} = k_{FLC}^d (G_{K36}(F_a, F_n, F_s) v(T) - [FLC])$$

Here, the total fractions of copies in each state (at any timepoint), i.e., F_a, F_n, F_s , can be computed as follows:

$$\text{Total fraction of active copies: } F_a = \frac{f_{a,d} + f_{a,nd}}{1 + f_{a,nd} + f_{n,nd} + f_{s,nd}}$$

$$\text{Total fraction of nucleated copies: } F_n = \frac{f_{n,d} + f_{n,nd}}{1 + f_{a,nd} + f_{n,nd} + f_{s,nd}}$$

$$\text{Total fraction of spread copies: } F_s = \frac{f_{s,d} + f_{s,nd}}{1 + f_{a,nd} + f_{n,nd} + f_{s,nd}}$$

Here, $g(T)$ represents the division rate, which undergoes a step change reduction in the cold. $g(T)$ is assumed to undergo a step reduction under FM and FS conditions, exactly as under constant cold conditions. The step change (factor of 40) is assumed to be the same under all three conditions. k_s represents the nucleation rate, computed using the VIN3 level as in (11), where the VIN3 level is itself computed using the LSCD model (10). At all timepoints, the current temperature is an input to the LSCD model. d_n represents the number of non-dividing copies produced at each division event (using the same simplified description as in (11)).

The rate of addition of H3K36me3 is assumed to be proportional to the function $G_{K36}(F_a, F_n, F_s)$:

$$G_{K36}(F_a, F_n, F_s) = \left(\frac{q(t)(r_a F_a + r_n F_n) + r_s F_s}{v(T)} \right).$$

$G_{K36}(F_a, F_n, F_s)$ represents the contribution to overall H3K36me3 addition from FLC sense transcriptional activity at FLC copies in different states, with the sense transcriptional activity dictated by both the H3K27me3 nucleation state (represented by r_a , r_n and r_s) and the antisense mediated repression (represented by $q(t)$). The multiplicative factors r_a , r_n and r_s represent the maximum transcription initiation rate for active, nucleated, and spread copies respectively. $v(T)$ represents the Pol II speed in the nucleation region, which is assumed to undergo a step change (reduction) during the cold. k_{K36me3}^d represents the turnover rate constant of H3K36me3. The H3K36me3 level is assumed to be normalised to its steady state level when $F_a = 1$, $v(T) = 1$, and $q(t) = 1$ (i.e., $G_{K36}(F_a, F_n, F_s)=1$).

The time-dependent multiplicative factor $q(t)$ captures the repression by the antisense mediated pathway. This factor has a basal value of 1 and decays exponentially with time to 0.5 in the cold and recovers exponentially with time in the post-cold. $q(t)$ undergoes a step reduction to a value of 0.05 whenever the temperature falls below 4°C. When the temperature subsequently rises above 4°C, $q(t)$ returns to its slow decaying value, which decays continuously irrespective of the temperature fluctuations.

Note that having the parameter $r_n > 0$ above means that copies in an H3K27me3 nucleated state can also contribute to H3K36me3 addition. This reflects the model assumption that these two modifications can coexist in the nucleation region at a single *FLC* copy during cold induced silencing, with the H3K36me3 levels being limited only by the level of sense transcription. This assumption is based on the ability of the VRN2-PRC2 complex (which mediates cold induced H3K27me3 accumulation at *FLC*) to methylate H3 histones even when they carry K36 methylation (15).

We describe *FLC* mRNA as an additional dynamical variable, whose production rate is proportional to $G_{K36}(F_a, F_n, F_s)v(T)$ – i.e. the same function $G_{K36}(F_a, F_n, F_s)$ described above, which captures the contribution to *FLC* sense initiation from antisense mediated repression and the different H3K27me3 states, but now multiplied by the Pol II speed in the nucleation region to cancel out the $v(T)$ factor in the denominator of $G_{K36}(F_a, F_n, F_s)$, so that the product represents a “transcriptional initiation rate”. k_{FLC}^d represents the turnover rate constant of *FLC* mRNA. The *FLC* mRNA level is also assumed to be normalised to its steady state level when $F_a = 1$, $v(T) = 1$, and $q(t) = 1$ (i.e., $G_{K36}(F_a, F_n, F_s)=1$).

Model for *COOLAIR* defective mutants: For simulating the *COOLAIR* defective mutants, the same model is used, but with the antisense mediated pathway assumed to be non-functional. This is captured by setting $q(t) = 1$ throughout the simulation.

Model for H3K27me3 Nucleation mutants: The basic model is used with the nucleation rate k_3 set to zero throughout the simulation. The initial conditions in this case are still allowed to have a non-zero fraction of H3K27me3 spread *FLC* copies, consistent with the NV level of H3K27me3 observed in cold-nucleation mutants including *vrn2-1* and *vin3-4* (12).

Model for H3K27me3 Spreading mutant: Here we modify the basic model to capture reactivation/loss of H3K27me3 nucleation. At each division event, a nucleated dividing copy is allowed to undergo three different scenarios (11):

- Reactivation, producing one active dividing copy and d_n active non-dividing copies.
- Spreading, producing one spread dividing copy and d_n spread non-dividing copies.
- Neither spreading nor reactivation, producing one nucleated dividing copy, $\beta_{nuc}d_n$ nucleated non-dividing copies, $\beta_{sprd}d_n$ spread non-dividing copies, and $\beta_{react}d_n$ active non-dividing copies.

$$\begin{aligned} \frac{df_{a,d}}{dt} &= -k_s f_{a,d} + \gamma g(T) f_{n,d} \\ \frac{df_{n,d}}{dt} &= k_s f_{a,d} - \delta g(T) f_{n,d} - \gamma g(T) f_{n,d} \\ \frac{df_{s,d}}{dt} &= \delta g(T) f_{n,d} \\ \frac{df_{a,nd}}{dt} &= d_n g(t) f_{a,d} - k_s f_{a,nd} + d_n \gamma g(T) f_{n,d} + \beta_{react} d_n (1 - \delta - \gamma) g(T) f_{n,d} \\ \frac{df_{n,nd}}{dt} &= k_s f_{a,nd} + \beta_{nuc} d_n (1 - \delta - \gamma) g(T) f_{n,d} \\ \frac{df_{s,nd}}{dt} &= d_n \delta g(T) f_{n,d} + d_n g(T) f_{s,d} + \beta_{sprd} d_n (1 - \delta - \gamma) g(T) f_{n,d} \\ \frac{d[H3K36me3]}{dt} &= k_{K36me3}^d (G_{K36}(F_a, F_n, F_s) - [H3K36me3]) \\ \frac{d[FLC]}{dt} &= k_{FLC}^d (G_{K36}(F_a, F_n, F_s) v(T) - [FLC]) \end{aligned}$$

Here γ represents the fraction of nucleated dividing copies undergoing reactivation and δ represents the fraction of nucleated dividing copies undergoing spreading, at each replication/division event. The parameters β_{nuc} , β_{sprd} , and β_{react} were computed numerically (see SI Table 1 of parameter values), using a Monte-Carlo approach to carry out five successive replication/division events starting from one nucleated copy (five divisions is consistent with our assumption of $d_n = 32$ (11)).

Processing simulation output:

The total fractions of copies in each state (at any timepoint) can be computed as follows from the simulation output:

$$\text{Total fraction of active copies: } F_a = \frac{f_{a,d} + f_{a,nd}}{1 + f_{a,nd} + f_{n,nd} + f_{s,nd}}$$

$$\text{Total fraction of nucleated copies: } F_n = \frac{f_{n,d} + f_{n,nd}}{1 + f_{a,nd} + f_{n,nd} + f_{s,nd}}$$

$$\text{Total fraction of spread copies: } F_s = \frac{f_{s,d} + f_{s,nd}}{1 + f_{a,nd} + f_{n,nd} + f_{s,nd}}$$

The total fractions of copies in each state are then used to compute the H3K27me3 levels as follows:

$$\text{NR H3K27me3 level: } K27_{NR} = p_{K27} ((0)F_a + (1)F_n + (1)F_s)$$

$$\text{Body H3K27me3 level: } K27_{Body} = p_{K27} ((0)F_a + (0)F_n + (1)F_s)$$

The factor p_{K27} is used for scaling the model output for comparison to ChIP-qPCR data. Similarly, a factor p_{K36} is multiplied when comparing H3K36me3 levels to the ChIP-qPCR data.

Comparing model predictions to experimental data under fluctuating temperature conditions:

In Figure S11(B,C,D), we compare the model predicted H3K36me3, H3K27me3, and *FLC* mRNA levels for *ColFRI* at the 2WT0 timepoint under fluctuating conditions to experimental data.

The model assumes that the *FLC* transcriptional shutdown in fluctuating conditions is mediated mainly by an enhanced antisense pathway. Hence, in the case of a *COOLAIR* defective mutant, this model would predict that the *FLC* transcriptional shutdown is mostly disrupted even in FM and FS conditions. Therefore, this model would predict an increase in H3K36me3 after 2W FM and FS conditions, similar to the increase predicted under constant cold conditions at the same timepoint (as shown in Figure 4). The experimental data for the TEX1.0 *FLCclean* mutant does show increased H3K36me3 across the locus under FM conditions (Fig. 3(D)), which is qualitatively consistent with the model prediction. This is similar to the increased H3K36me3 across the locus observed for all three *COOLAIR* defective mutants after 2W cold (Fig. 2(B)). However, under FS conditions, the data shows a reduction in H3K36me3 (although this reduction is significantly attenuated compared to *ColFRI* – Figure S9F). This indicates that there may be additional factors driving the transcriptional shutdown under FS conditions that are not captured by this simple model,

which require further experimental analysis of chromatin state changes under fluctuating temperatures to dissect.

Note: Defining parameter values under fluctuating temperature conditions

The instantaneous temperature input affects the parameters in the LSCD model of VIN3 dynamics and the rate of VIN3 mediated nucleation as described in (10). The parameter $q(t)$, representing the antisense mediated repression undergoes step changes under the fluctuating temperature conditions as defined above. $g(T)$, representing the division rate and $v(T)$, representing the Pol II speed in the nucleation region, are set to the same, constant value under all three cold conditions (constant, FM, FS). See Table S1 for details.

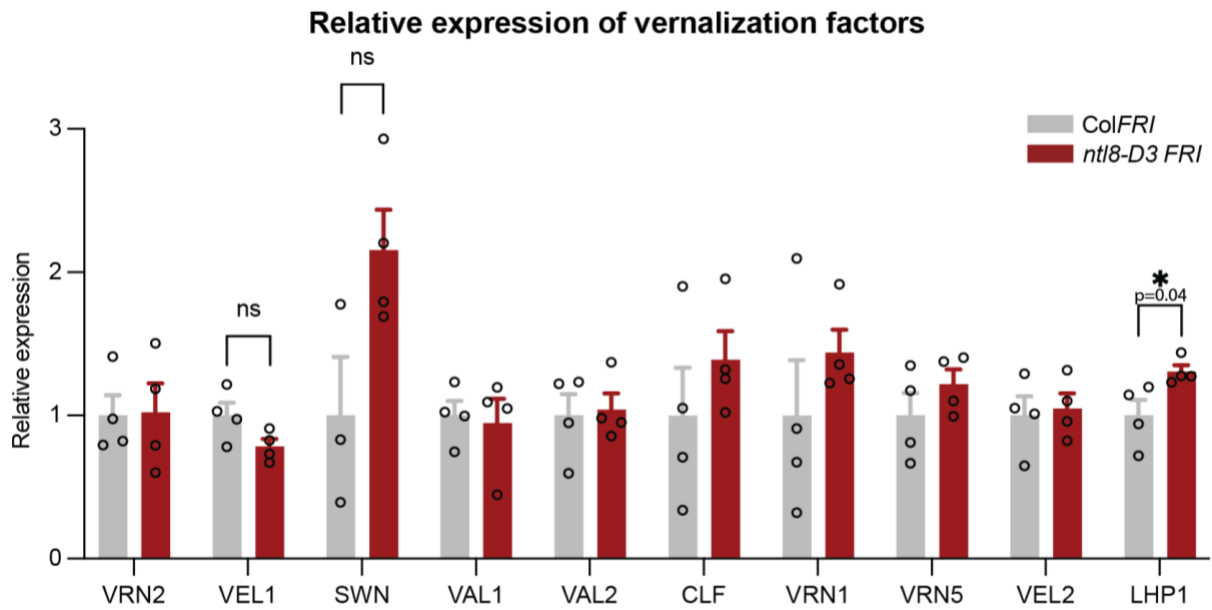


Fig. S1. Relative expression of other factors involved in vernalization. Expression of vernalization factors in *ntl8-D3 FRI* compared to *ColFRI* in non-vernalized conditions. Data are presented as the mean \pm s.e.m ($n \geq 3$). Asterisks indicate significant different ($p \leq 0.05$, two-tailed t test). n.s., not significant. Each open circle represents a biological replicate.

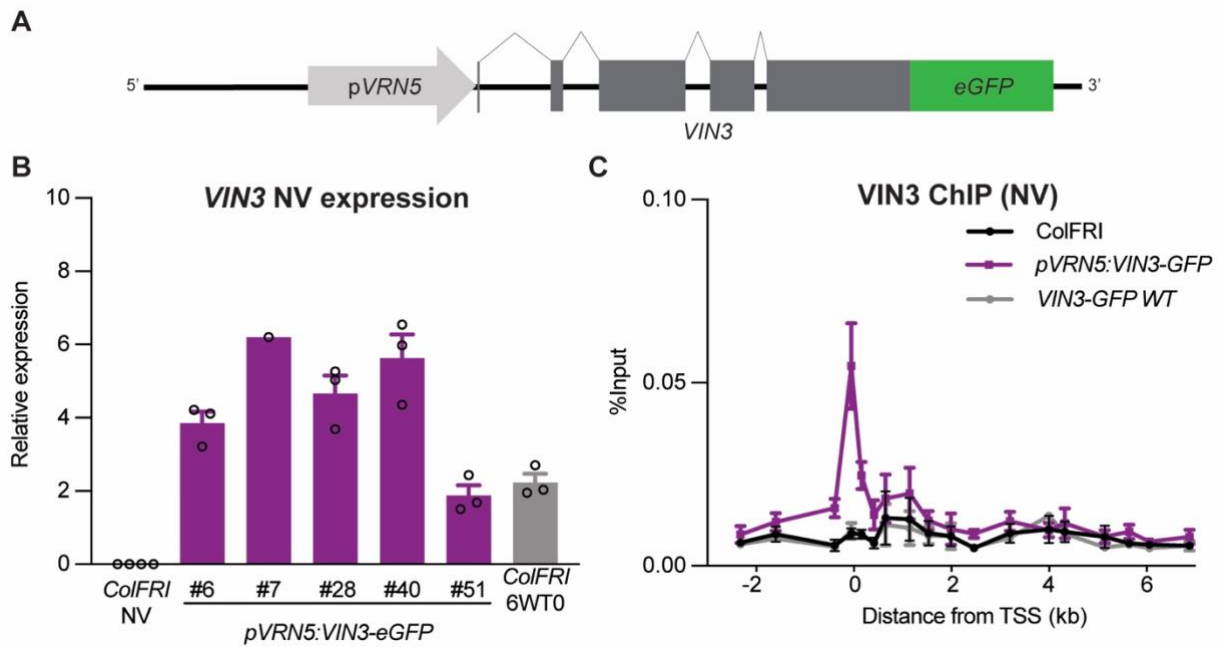


Fig. S2. Constitutive expressed VIN3 binds the nucleation region at *FLC*. (A) Schematic of the construct used to generate transgenic lines that express VIN3 in the absence of cold. The *VIN3* promoter was exchanged with the promoter sequence of *VRN5* (*pVRN5*). (B) Expression of *VIN3* in non-vernalized conditions (NV), *VIN3* expression in *ColFRI* after six weeks of vernalization (6WT0) is shown for comparison. Data are presented as the mean \pm s.e.m relative to the geometric mean of *PP2A* and *ACTIN*. Each open circle represents a biological replicate. The numbers under the bars refer to individual transgenic lines. (C) *VIN3*-eGFP ChIP-qPCR enrichment at *FLC* at NV. Data are shown as percentage input. Non-transgenic *ColFRI* plants were used as a negative control sample. Error bars represent mean \pm s.e.m. (n = 3 biological replicates).

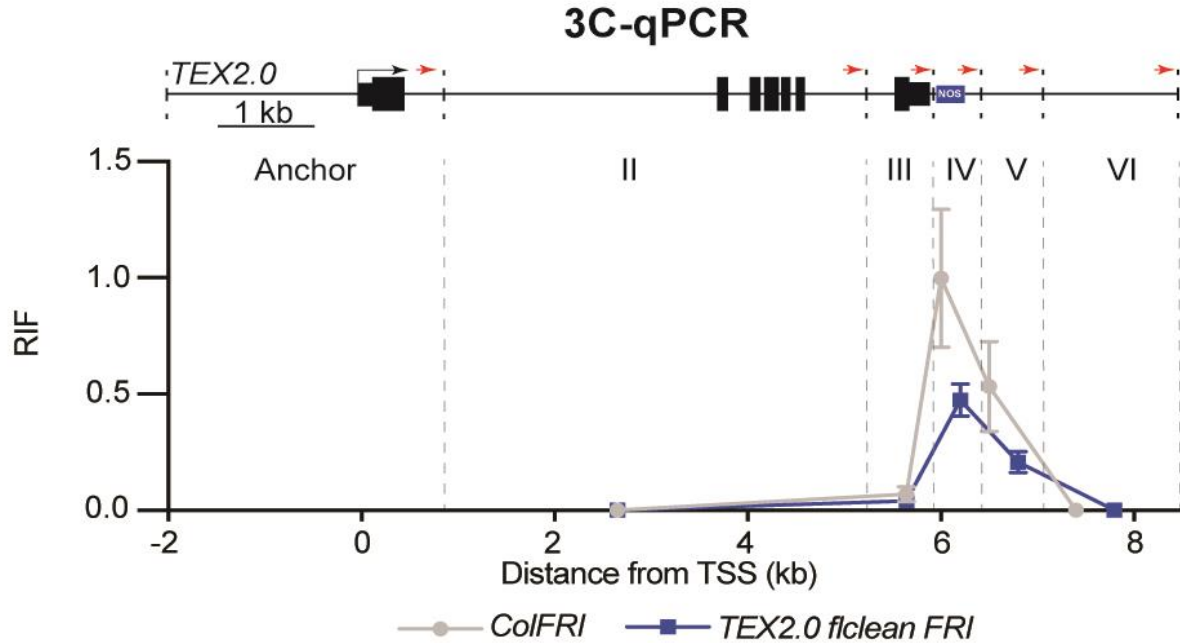


Fig. S3. Gene-loop is disrupted in *TEX2.0*. Quantitative 3C over the *FLC* locus in 10-day-old *ColFRI* and *TEX2.0 flclean FRI* with BamHI and BglII (similar to Fig. 1G). A schematic of the *TEX2.0* transgene is shown above. BamHI and BglII restriction sites are indicated with dotted lines, and the respective regions are numbered with Roman numerals. The insertion of the NOS sequence does not result in additional 3C fragments when assayed with BglII and BamHI. Red arrows indicate the primers' location for 3C-qPCR. The region around the *FLC* transcription start site was used as the anchor region in the 3C analysis. The data shows the relative interaction frequencies (RIF) and are the average of at least seven biological replicates. Data are presented as the mean \pm s.e.m. ($n \geq 7$). The midpoint of the assayed 3C fragments is plotted.

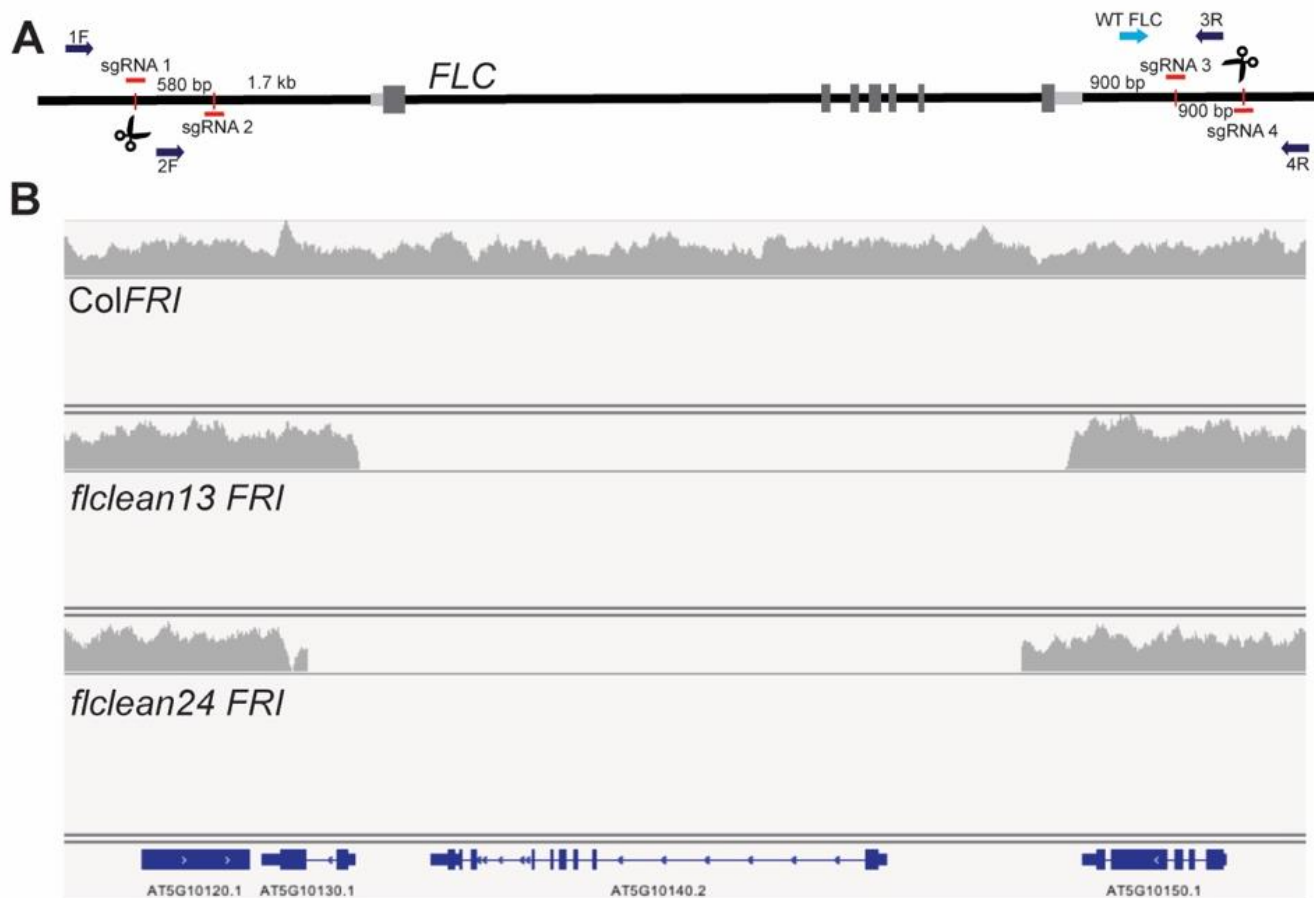


Fig. S4. CRISPR/Cas9 mediated generation of *FLC* deletion lines (*FLCclean*). (A) Schematic representation of the *FLC* locus with locations of sgRNA target sites (Red) and primer binding sites for genotyping (Blue). The size numbers refer to the region at 5' and 3' end of *FLC* removed in the *FLCclean* lines. (B) Integrative Genomics Viewer (IGV) screenshot of *FLC* genomic region showing read coverage of whole genome DNA sequencing in ColFRI and two CRISPR *FLCclean* lines. The *FLCclean* lines were created through removal of the whole *FLC* locus with either sgRNA1 and 3 (*FLCclean13*) or sgRNA 2 and 4 (*FLCclean24*).

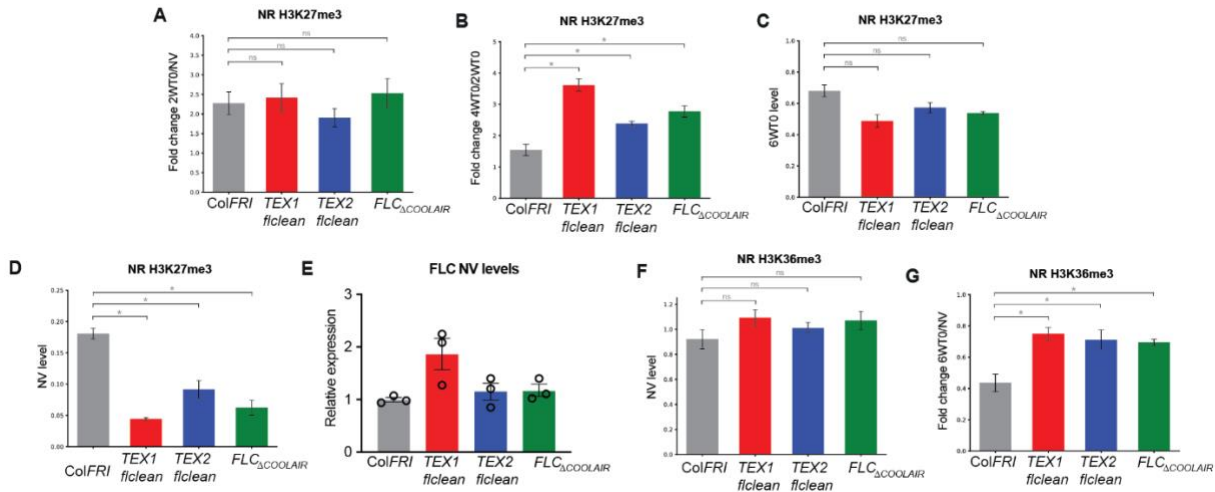


Fig. S5. Quantitative analysis of antisense role in histone modification dynamics. All comparisons shown consist of comparing the mean levels over three nucleation region primers between *ColFRI* to each of the defective *COOLAIR* lines (See supplementary information for details of primers). In cases where the qualitative trends were clear and consistent across the three defective *COOLAIR* lines, a one-tailed Student's t-test was used for each comparison. Error bars represent s.e.m. (n = 3 biological replicates). In (A), where there was no clear trend, a two-tailed Student's t-test was used. In all cases, the Bonferroni correction was used to adjust the significance level from $\alpha = 0.05$ to $\alpha = 0.0167$ (for three comparisons). (*) indicates $P < 0.0167$; ns indicates no significance ($P \geq 0.0167$). (A) Fold change (increase) of H3K27me3 in the nucleation region during first 2 weeks of cold treatment (2WT0/NV) is not significantly different between *ColFRI* and the defective *COOLAIR* lines. (B) Fold change (increase) of H3K27me3 in the nucleation region during the 2WT0 to 4WT0 period is significantly higher in the *COOLAIR* lines. (C) H3K27me3 levels at 6WT0 are not significantly lower in the defective *COOLAIR* lines. (D) NV level of H3K27me3 in the nucleation region is significantly higher in *ColFRI*. (E) *FLC* expression in 10 days old seedlings before cold exposure in *ColFRI* and the three defective *COOLAIR* lines; *TEX1*, *TEX2*, and *FLC Δ COOLAIR*. Unspliced RNA was measured and is shown relative to *UBC* and *ColFRI*. Error bars represent s.e.m. (n = 3 biological replicates). (F-G) Similar analysis as in (A-D). NV level of H3K36me3 is not significantly higher in the defective *COOLAIR* lines (F). The fold change in H3K36me3 over 6W of cold treatment indicates significantly smaller changes in H3K36me3 in the defective *COOLAIR* lines (G).

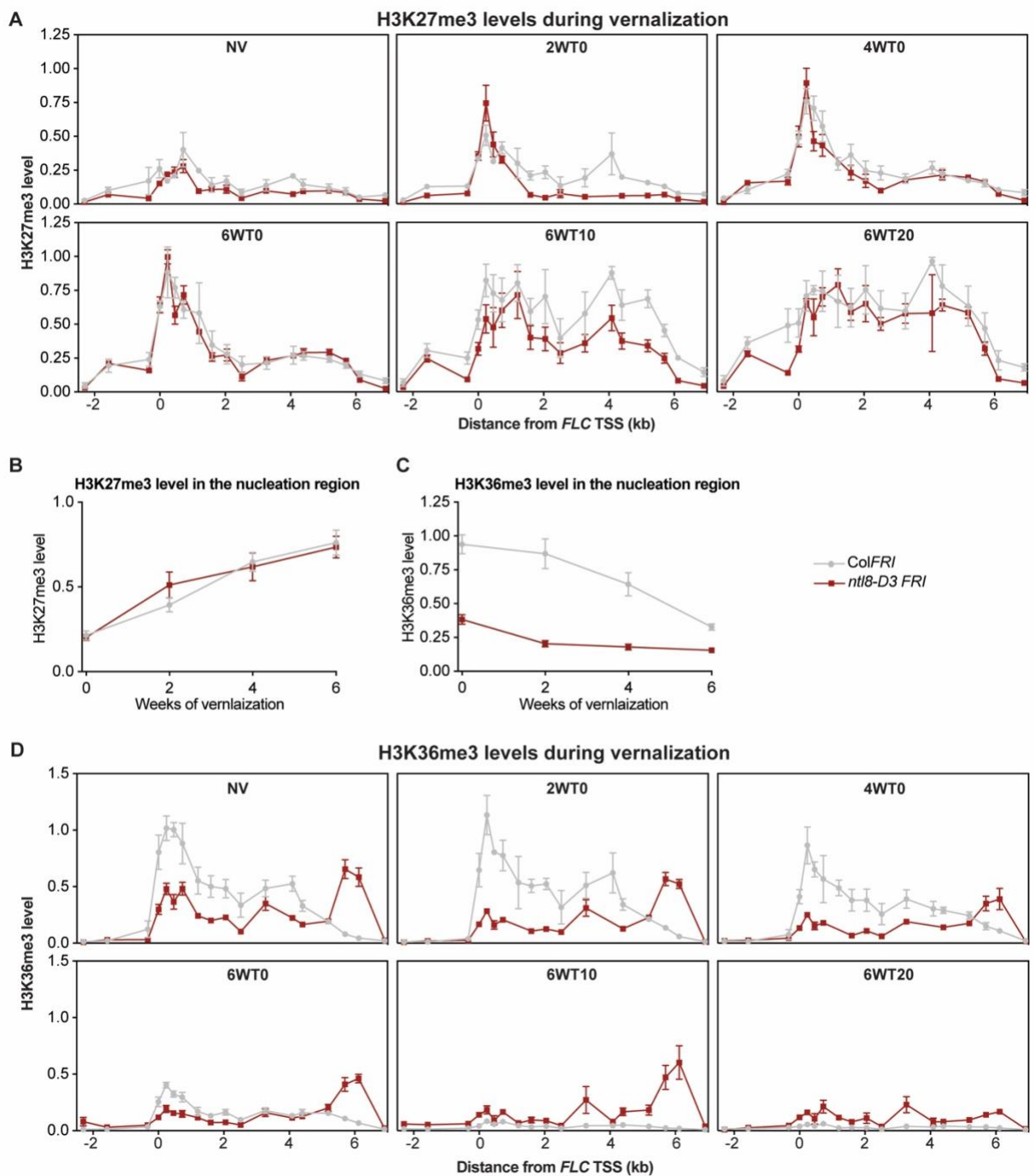


Fig. S6. Polycomb repression of *FLC* is not inhibited by hyperactive antisense pathway in *ntl8-D3*. (A) H3K27me3 ChIP in *ColFRI* and *ntl8-D3 FRI* across the *FLC* locus before, during, and after vernalization. H3K27me3 levels are expressed as relative to H3 and to the levels at the positive control gene *STM*. Data are presented as the mean \pm s.e.m. ($n \geq 3$). (B) H3K27me3 levels in the nucleation region in *ColFRI* and *ntl8-D3 FRI* during vernalization. The levels were calculated by averaging over three primers in the *FLC* nucleation region. (C) H3K36me3 levels in the nucleation region in *ColFRI* and *ntl8-D3 FRI* during vernalization. The levels were calculated as in B. (D) H3K36me3 ChIP in *ColFRI* and *ntl8-D3 FRI* across the *FLC* locus before, during, and after vernalization. H3K36me3 levels are expressed as relative to H3 and to the levels at the positive control gene *Actin*. Data are presented as the mean \pm s.e.m. ($n \geq 3$).

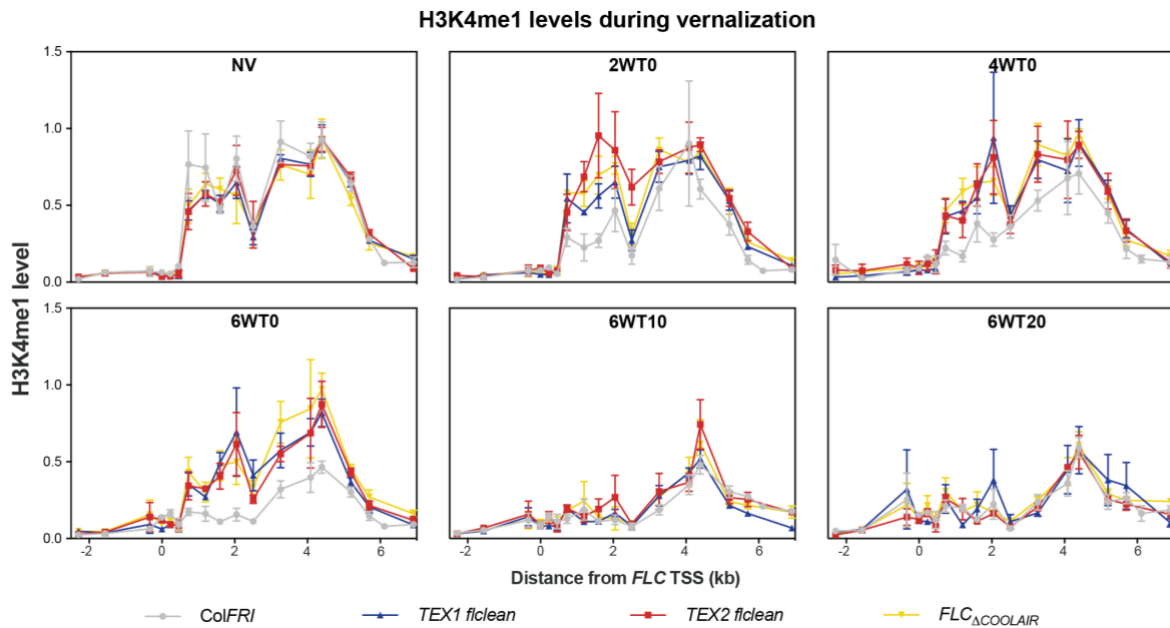


Fig. S7. H3K4me1 removal during the cold is attenuated in COOLAIR defective lines. H3K4me1 ChIP in *ColFRI* and the three COOLAIR mutant lines; *TEX1*, *TEX2*, and *FLC Δ COOLAIR* across the *FLC* locus before, during, and after vernalization. Data are presented as the mean \pm s.e.m. ($n \geq 3$).

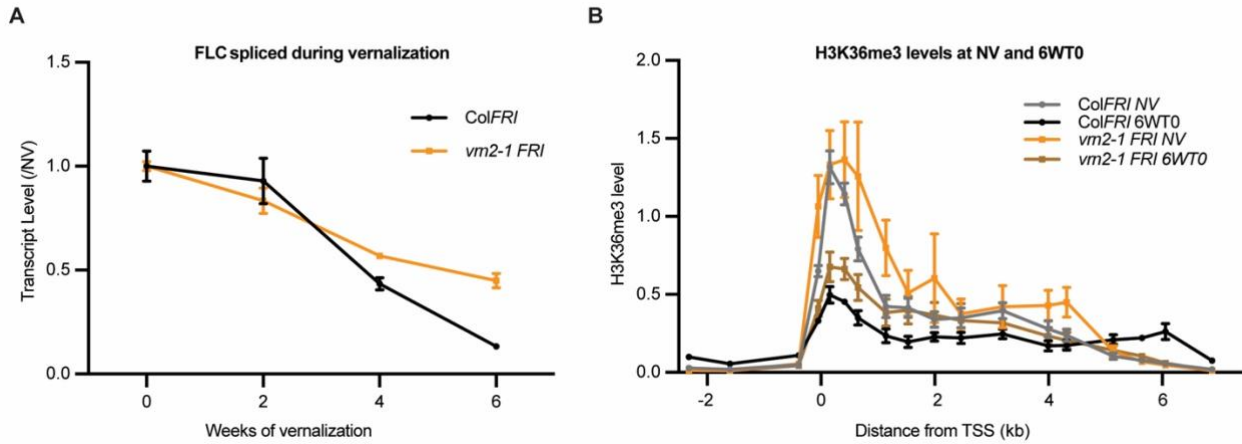


Fig. S8. *FLC* repression is only partially disrupted in *vrn2-1 FRI*. (A) *FLC* spliced levels and (B) H3K36me3 levels during vernalization in *ColFRI* and *vrn2-1 FRI*. (A) *FLC* spliced data shown relative to RNA levels in non-vernalized conditions (0 weeks of vernalization). (B) ChIP-qPCR data for H3K36me3 is normalized to H3 and shown relative to H3 normalized H3K36me3 levels at *ACTIN*. Data are presented as the mean \pm s.e.m. ($n \geq 3$). Reproduced from (12).

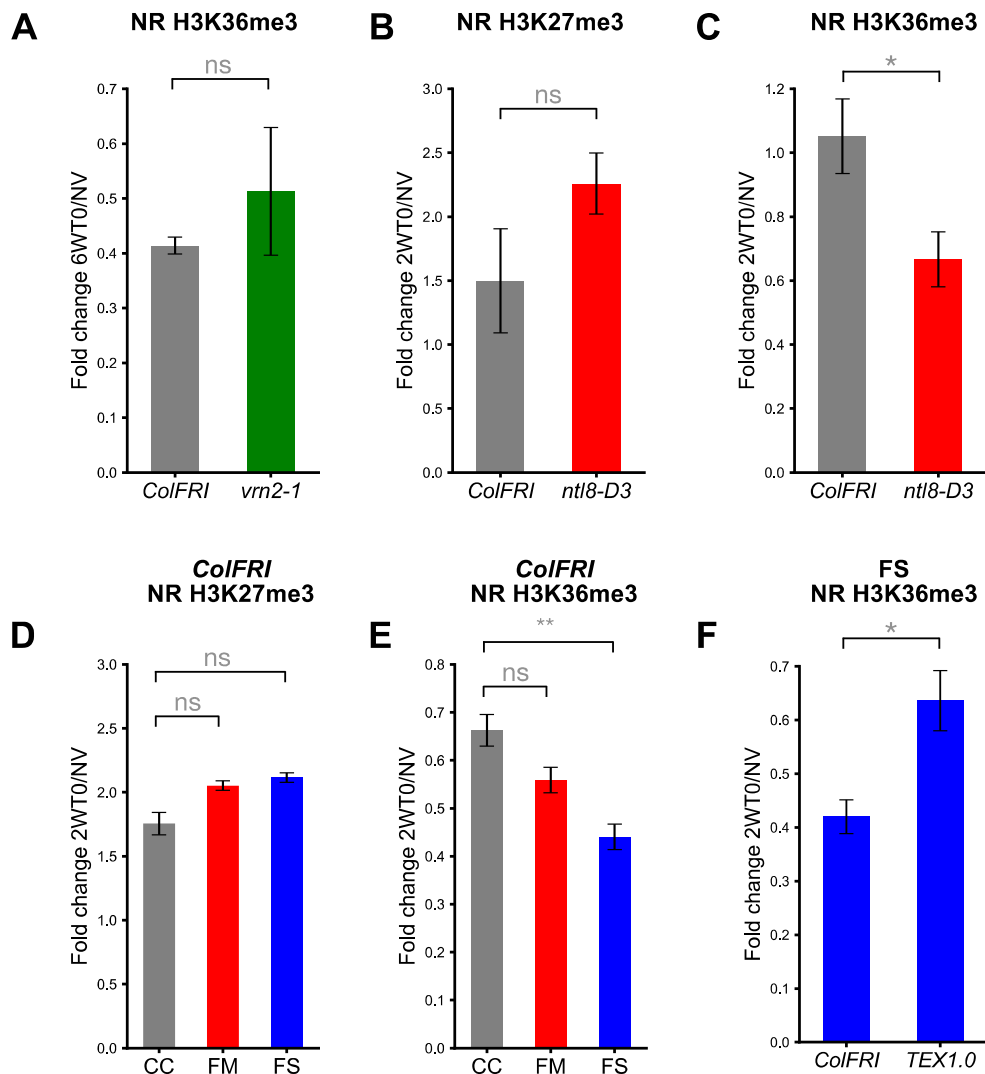


Fig. S9. Fold change comparisons for changes in nucleation region H3K36me3 and H3K27me3. This analysis is based on ChIP-qPCR time course data presented in Figs. 1,2. Error bars represent mean \pm s.e.m. ($n \geq 3$). All comparisons shown consist of comparing fold changes in the mean levels over three nucleation region primers in the indicated genotypes between different periods of cold and non-vernalized conditions (see supplementary information for details of primers). In all cases, the data showed clear trends, so a one-tailed Student's t-test was used for each comparison. In (A-C) and (F), a significance level of $\alpha = 0.05$ was used. (*) indicates $P < 0.05$; ns indicates no significance ($P \geq 0.05$). In (D), the Bonferroni correction was used to adjust the significance level from $\alpha = 0.05$ to $\alpha = 0.025$ (for two comparisons). ns indicates no significance ($P \geq 0.025$). In (E), the Bonferroni correction was used to adjust the significance level from $\alpha = 0.01$ to $\alpha = 0.005$ (for two comparisons). (**) indicates $P < 0.005$; ns indicates no significance ($P \geq 0.005$). (A) Comparison of NR H3K36me3 fold changes after 6 weeks cold (6WTO) in *ColFRI* and *vrn2-1*. (B) Comparison of NR H3K27me3 fold changes after 2 weeks cold

(2WT0) in *ColFRI* and *ntl8-D3*. **(C)** Comparison of NR H3K36me3 fold changes after 2 weeks cold (2WT0) in *ColFRI* and *ntl8-D3*. **(D)** Comparison of NR H3K27me3 fold changes after 2 weeks cold (2WT0) in *ColFRI* under different cold conditions – constant cold (CC), fluctuating mild (FM), and fluctuating strong (FS). **(E)** Comparison of NR H3K36me3 fold changes after 2 weeks cold (2WT0) in *ColFRI* under different cold conditions – constant cold (CC), fluctuating mild (FM), and fluctuating strong (FS). **(F)** Comparison of NR H3K36me3 fold changes after 2 weeks (2WT0) under FS conditions in *ColFRI* and *TEX1.0*.

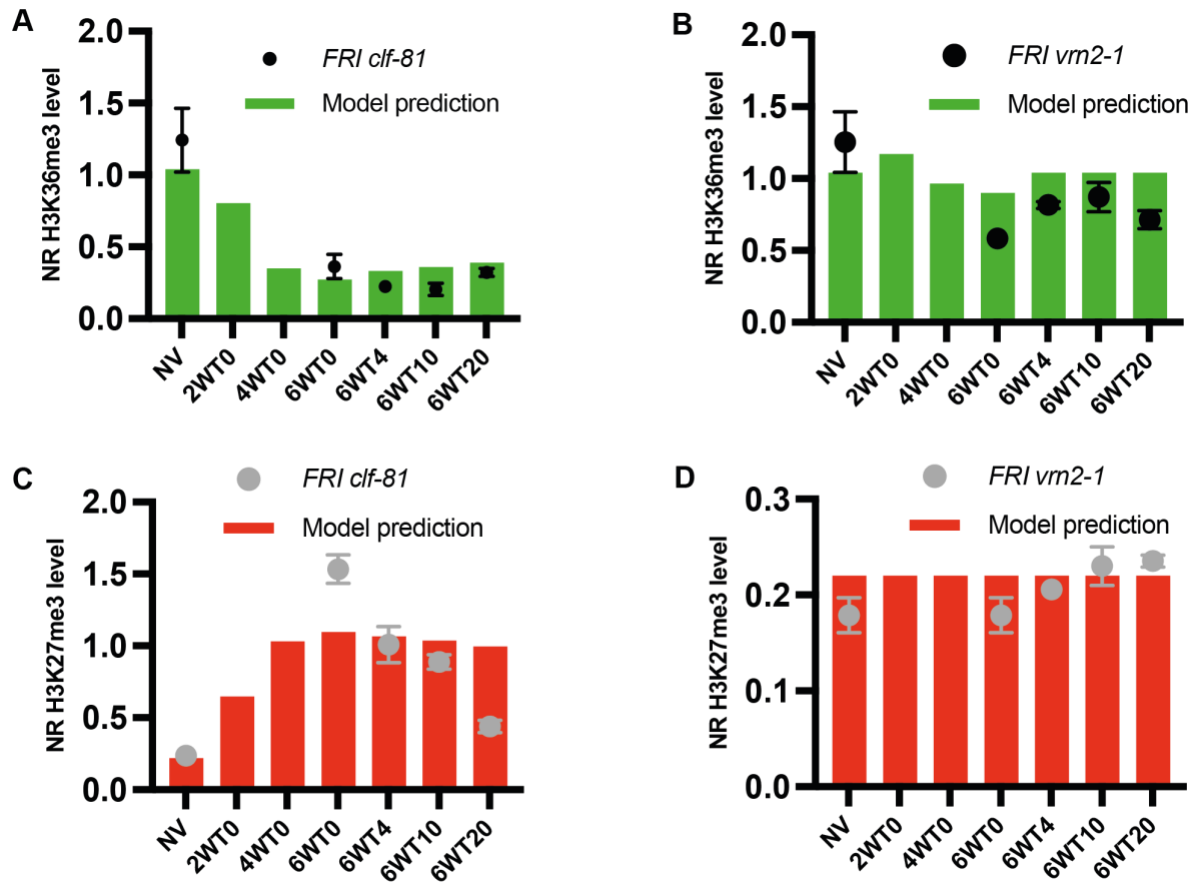
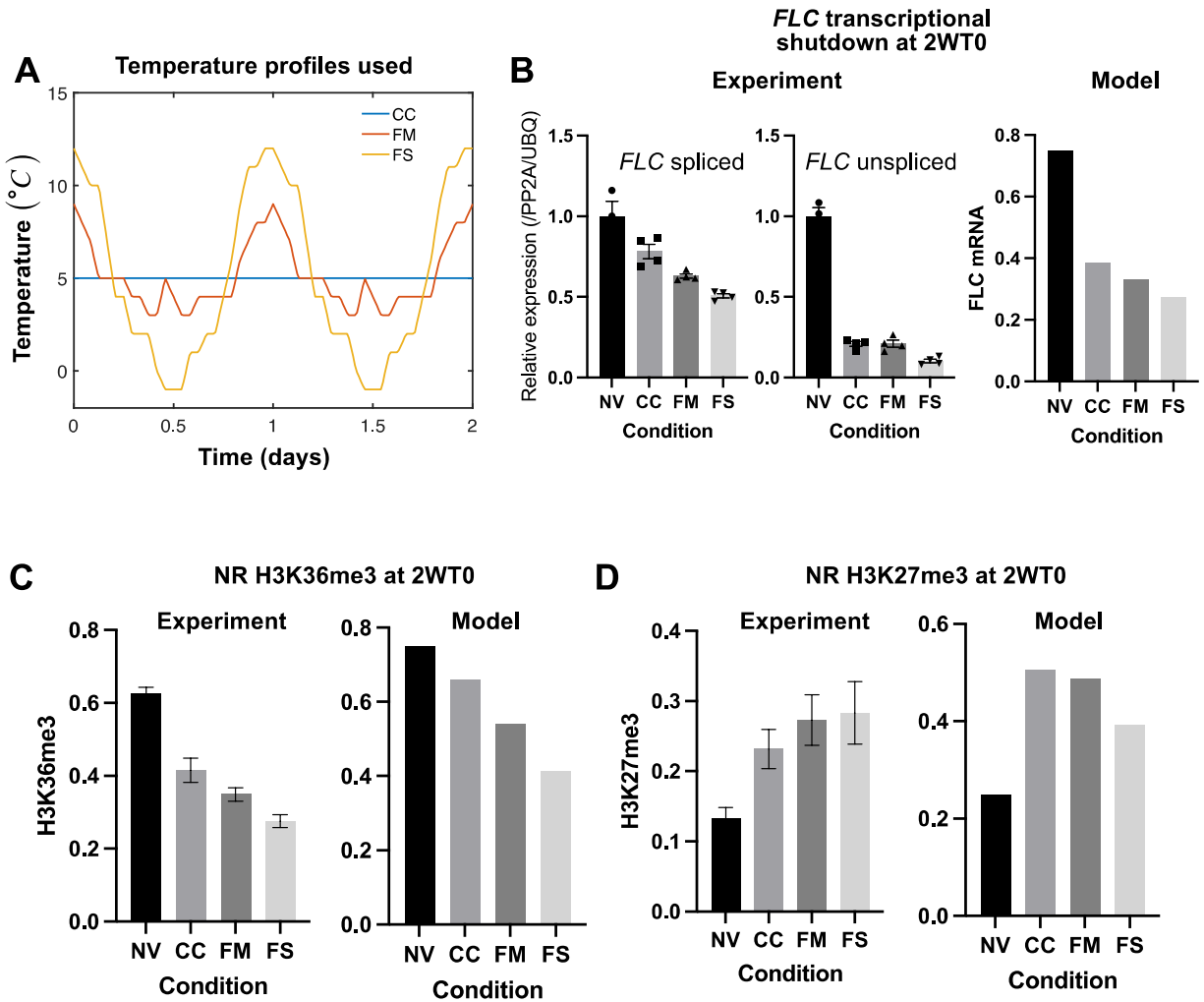


Figure S10. Model predictions of impact of vernalization mutants on histone dynamics.

(A-D) Time course predictions from the mathematical model for other vernalization mutants: an H3K27me3 nucleation mutant, and a spreading mutant. The predictions are compared to previously published ChIP-qPCR time course data presented in (12).



Caption for Figure S11: Fast timescale response of the antisense mediated repression pathway to temperature fluctuations can capture experimentally observed changes under fluctuating temperature conditions. (A) Temperature profiles used in the fluctuating temperature experiments. **(B)** Comparison of experimentally measured (left) and model predicted (right) changes in *FLC* transcriptional output in *ColFRI* after 2W constant cold (CC), 2W fluctuating mild (FM), or 2W fluctuating strong (FS) conditions. The experimentally measured levels are normalised to the mean NV level. **(C)** Comparison of experimentally measured (left) and model predicted (right) changes in nucleation region H3K36me3 in *ColFRI* after 2W constant cold (CC), 2W fluctuating mild (FM), or 2W fluctuating strong (FS) conditions. **(D)** Comparison of experimentally measured (left) and model predicted (right) changes in nucleation region H3K27me3 in *ColFRI* after 2W constant cold (CC), 2W fluctuating mild (FM), or 2W fluctuating strong (FS) conditions.

Table S1. Model parameter values

Parameter	Description	Value	Reference
k_s	Rate constant of H3K27me3 nucleation (day ⁻¹)	Computed as in (11), with $p_{s2} = 0.007 \text{ day}^{-1}\text{C}^{-2}$	(10,11)
$g(T)$	Temperature dependent growth rate (day ⁻¹)	0.4 for $T = 22^\circ\text{C}$ 0.01 for $T = 5^\circ\text{C}$ Constant, FM, and FS conditions	(11)
d_n	Number of non-dividing copies produced per division of a dividing copy	32	(11)
δ	Fraction of H3K27me3 nucleated dividing copies undergoing spreading	0.0025	This allows for a very small fraction undergoing H3K27me3 spreading, even in a spreading mutant. Consistent with very low levels of H3K27me3 spreading observed in (12).
γ	Fraction of H3K27me3 nucleated dividing copies undergoing reactivation during a replication/division event	0.03	Chosen to produce ~30% reactivation after 12 replication/division events starting from a single nucleated copy. This is based on the analysis of <i>FLC</i> reactivation in a spreading mutant in (12)

β_{sprd}	Fraction of H3K27me3 spread non-dividing copies produced during replication of a nucleated copy in the spreading mutant model	0.0121	Numerically estimated from the same Monte Carlo simulation described above.
β_{react}	Fraction of non-dividing copies that have lost H3K27me3 nucleation, produced during replication of a nucleated copy in the spreading mutant model	0.1402	Numerically estimated from the same Monte Carlo simulation described above.
$q(t)$	Time-dependent multiplicative factor that captures repression by the antisense mediated pathway.	$q(t) = 1$ before cold (and during cold when simulating COOLAIR defective mutants) <hr/> $q(t) = 0.5(1 + e^{-\alpha_1(t-10)})$ during cold (beginning at 10 days), for $T \geq 4^\circ\text{C}$ <hr/> $q(t) = 1 - (1 - 0.5(1 + e^{-\alpha_1(42)}))e^{-\alpha_2(t-52)}$ during post-cold (beginning at 52 days) <hr/> $q(t) = 0.05$ for $T < 4^\circ\text{C}$	This study
α_1	Rate constant of increasing antisense mediated repression during cold (day^{-1})	0.08	This study
α_2	Rate constant of decreasing antisense mediated repression during post-cold (day^{-1})	0.12	This study
$v(T)$	Temperature dependent RNA Pol II speed in the nucleation region	1 for $T = 22^\circ\text{C}$ 0.6 for $T = 5^\circ\text{C}$ Constant, FM, and FS conditions	This study
r_a	Maximum transcription initiation rate for active	1	This study

	copies (assumed normalised to rate at active copies)		
r_n	Maximum transcription initiation rate for nucleated copies (assumed normalised to rate at active copies)	0.3	This study
r_s	Maximum transcription initiation rate for spread copies (assumed normalised to rate at active copies)	0.025	This study
k_{K36me3}^d	Turnover rate constant of H3K36me3	1.21 day^{-1}	Consistent with the half-life of H3K36me2 (0.571 day) estimated in (20)
k_{FLC}^d	Turnover rate constant of <i>FLC</i> mRNA	2.78 day^{-1}	Consistent with a half-life of 6 hr as estimated in (21).
p_{K36}	Scaling parameter for comparing model output to ChIP-qPCR data	1.3 for <i>FRI clf-2</i> and <i>FRI vrn2-1</i> (Data from (12)) 1.3 for <i>ColFRI</i> , and <i>COOLAIR</i> defective mutants (Data from this study)	This study
p_{K27}	Scaling parameter for comparing model output to ChIP-qPCR data	1.1 for <i>FRI clf-2</i> and <i>FRI vrn2-1</i> (Data from (12)) 0.7 for <i>ColFRI</i> , and <i>COOLAIR</i> defective mutants (Data from this study)	This study

Table S2. Fluctuating temperature profiles input to model (matching conditions used in fluctuating temperature experiments). The temperature input is linearly interpolated between the hourly timepoints shown.

Time (h)	FM Conditions (°C)	FS Conditions (°C)
0	9	12
1	8	11
2	7	10
3	5	10
4	5	7
5	5	4
6	5	4
7	4	2
8	4	2
9	3	2
10	3	0
11	5	-1
12	4	-1
13	3	-1
14	3	1
15	4	1
16	4	2
17	4	2
18	4	4
19	4	6
20	6	9
21	7	11
22	8	11
23	8	12
24	9	12

Dataset S1. List of primers used in this study.

SI References

1. Y. Zhao, et al., Natural temperature fluctuations promote COOLAIR regulation of *FLC*. *Genes Dev.* **35**, 888–898 (2021).
2. X. Luo, T. Chen, X. Zeng, D. He, Y. He, Feedback regulation of *FLC* by *FLOWERING LOCUS T (FT)* and *FD* through a 5' *FLC* promoter region in Arabidopsis. *Mol. Plant* **12**, 285–288 (2019).
3. I. Lee, S. D. Michaels, A. S. Masshardt, The late-flowering phenotype of *FRIGIDA* and mutations in *LUMINIDEPENDENS* is suppressed in the Landsberg erecta strain of Arabidopsis. *The Plant* (1994).
4. T. Csorba, J. I. Questa, Q. Sun, C. Dean, Antisense COOLAIR mediates the coordinated switching of chromatin states at *FLC* during vernalization. *Proc. Natl. Acad. Sci. U. S. A.* **111**, 16160–16165 (2014).
5. J. I. Questa, J. Song, N. Geraldo, H. An, C. Dean, Arabidopsis transcriptional repressor VAL1 triggers Polycomb silencing at *FLC* during vernalization. *Science* **353**, 485–488 (2016).
6. M. S. Box, V. Coustham, C. Dean, J. S. Mylne, Protocol: A simple phenol-based method for 96-well extraction of high quality RNA from Arabidopsis. *Plant Methods* **7**, 7 (2011).
7. E. Franco-Echevarría, et al., Distinct accessory roles of Arabidopsis VEL proteins in Polycomb silencing. *Genes. Dev* (2023).
8. P. Crevillén, C. Sonmez, Z. Wu, C. Dean, A gene loop containing the floral repressor *FLC* is disrupted in the early phase of vernalization. *EMBO J.* **32**, 140–148 (2013).
9. M. Louwers, E. Splinter, R. van Driel, W. de Laat, M. Stam, Studying physical chromatin interactions in plants using Chromosome Conformation Capture (3C). *Nat. Protoc.* **4**, 1216–1229 (2009).
10. R. L. Antoniou-Kourouniotti, et al., Temperature Sensing Is Distributed throughout the Regulatory Network that Controls *FLC* Epigenetic Silencing in Vernalization. *Cell Syst* **7**, 643–655.e9 (2018).
11. J. I. Questa, et al., Noncoding SNPs influence a distinct phase of Polycomb silencing to destabilize long-term epigenetic memory at Arabidopsis *FLC*. *Genes Dev.* **34**, 446–461 (2020).
12. H. Yang, et al., Distinct phases of Polycomb silencing to hold epigenetic memory of cold in Arabidopsis. *Science* **357**, 1142–1145 (2017).
13. E. J. Finnegan, E. S. Dennis, Vernalization-induced trimethylation of histone H3 lysine 27 at *FLC* is not maintained in mitotically quiescent cells. *Curr. Biol.* **17**, 1978–1983 (2007).
14. H. Yang, M. Howard, C. Dean, Antagonistic roles for H3K36me3 and H3K27me3 in the cold-induced epigenetic switch at Arabidopsis *FLC*. *Curr. Biol.* **24**, 1793–1797 (2014).
15. F. W. Schmitges, et al., Histone methylation by PRC2 is inhibited by active chromatin marks. *Mol. Cell* **42**, 330–341 (2011).
16. Y. Zhao, R. L. Antoniou-Kourouniotti, G. Calder, C. Dean, M. Howard, Temperature-dependent growth contributes to long-term cold sensing. *Nature* **583**, 825–829 (2020).
17. P. Zhu & C. Dean, Reply to: Cold induction of nuclear FRIGIDA condensation in Arabidopsis. *Nature* (2023).

18. H. Yang, M. Howard, C. Dean, Physical coupling of activation and derepression activities to maintain an active transcriptional state at *FLC*. *Proc. Natl. Acad. Sci. U. S. A.* **113**, 9369–9374 (2016).
19. N. Fong, T. Saldi, R. M. Sheridan, M. A. Cortazar, D. L. Bentley, RNA Pol II Dynamics Modulate Co-transcriptional Chromatin Modification, CTD Phosphorylation, and Transcriptional Direction. *Mol. Cell* **66**, 546–557.e3 (2017).
20. B. M. Zee, *et al.*, In vivo residue-specific histone methylation dynamics. *J. Biol. Chem.* **285**, 3341–3350 (2010).
21. R. Ietswaart, S. Rosa, Z. Wu, C. Dean, M. Howard, Cell-Size-Dependent Transcription of *FLC* and Its Antisense Long Non-coding RNA COOLAIR Explain Cell-to-Cell Expression Variation. *Cell Syst* **4**, 622-635.e9 (2017).